SIAM J. Applied Dynamical Systems
Vol. 17, No. 4, pp. 2516–2543

An Operational Definition of Phase Characterizes the Transient Response of Perturbed Limit Cycle Oscillators*

Dan Wilson† and Bard Ermentrout‡

Abstract. Phase reduction is an essential tool used in the study of perturbed limit cycle oscillators. Usually, phase is defined with respect to some asymptotic limit, often making phase reduction's ability to predict transient behavior during the approach to a limit cycle inadequate. In this work, we present an operational notion of phase, defined with respect to a distinct feature of the oscillator, for example, the timing of a periodically firing neuron's action potential. We derive relationships between standard and operational phase reduction in order to make comparisons between these two approaches. In theoretical and numerical examples, we show how operational phase reduction accurately predicts both the asymptotic and transient behavior due to perturbations without relying on the notion of higher order phase response curves which are valid only for specific perturbations. Furthermore, we develop a strategy for direct measurement of the necessary terms of the operational phase reduction when the full dynamical equations are unknown.

Key words. phase reduction, isostable, isochron, neuroscience, noise, limit cycle

AMS subject classifications. 70G60, 70K05, 92B25, 34E05

DOI. 10.1137/17M1153261

1. Introduction.

Many biological systems exhibit periodicity at various levels of organizational complexity, from the circadian oscillations that regulate the 24-hour cycles of entire organisms [47] to the synchronous periodic firing of individual neurons that give rise to measurable brain rhythms [1], [3]. However the underlying mechanisms behind these oscillations are often obscured by a lack of information about the system behavior, where it is simply not possible to measure all of the important variables that give rise to the observed oscillatory behavior. Despite this limitation, useful analysis can still be performed by using phase reduction [47], [17], [22], [10], by which the dynamics of a limit cycle oscillator of the form

$$\frac{dx}{dt} = F(x) + G(t), \quad x \in \mathbb{R}^N, \tag{1}$$

can be represented by the single variable system:

$$\frac{d\theta}{dt} = \omega + \mathcal{Z}(\theta)^T G(t), \qquad \theta \in \mathbb{S}^1. \tag{2}$$

Here, F gives the nominal unperturbed dynamics, $\theta \in [0, 2\pi)$ represents the asymptotic phase of an oscillator, giving a general sense of its state near the periodic orbit, $\omega = 2\pi/T$ is the

*Received by the editors October 23, 2017; accepted for publication (in revised form) by H. Osinga August 29, 2018; published electronically October 30, 2018.
http://www.siam.org/journals/siads/17-4/M115326.html
Funding: This work was supported by National Science Foundation grant NSF-1602841.
†Department of Electrical Engineering and Computer Science, University of Tennessee, Knoxville, TN 37996 (dwilso81@utk.edu).
‡Department of Mathematics, University of Pittsburgh, Pittsburgh, PA 15213 (bard@math.pitt.edu).

natural frequency where T is the period of oscillation, and $\mathcal{Z}(\theta) \in \mathbb{R}^N$ is the infinitesimal phase response curve (iPRC) to external perturbations $G(t) \in \mathbb{R}^N$. A key aspect of (2) is the resulting reduction in dimensionality and complexity, allowing further analysis to predict more complicated behavior such as entrainment, phase locking, and synchronization [10], [47], [43], [45], [2]. Phase reduction is particularly useful in experimental systems because all of its required terms can be inferred using the direct method [18], [28], whereby a series of perturbations at known phases are applied, the resulting phase changes are estimated, and the iPRC is inferred from the resulting data.

As mentioned above, the phase coordinate from (2) is determined by the oscillator's asymptotic approach to the limit cycle. For all locations on the limit cycle, $\dot{\theta} = \omega$ and the location corresponding to $\theta = 0$ can be chosen arbitrarily. The notion of asymptotic phase can be extended to the basin of attraction of the limit cycle using isochrons [47], [14]. For example, for some $X(0)$ on the limit cycle of (1), the associated isochron is defined to be the set of all initial conditions $Y(0)$ for which

$$\lim_{t\to\infty} ||X(t) - Y(t)|| = 0, \tag{3}$$

where $||\cdot||$ can be any norm. However, in many cases we are not specifically interested in the asymptotic behavior and are more concerned with aspects of the transient behavior. In other cases, the oscillator might be continuously perturbed, never reaching its limit cycle and making the notion of asymptotic phase difficult to interpret. As a concrete example, consider the Wang–Buzsaki model of neural behavior [40], with the addition of an adaptation current [7],

$$\begin{aligned} C\dot{V} &= -g_{\mathrm{Na}} m_\infty^3 h(V - E_{\mathrm{Na}}) - g_{\mathrm{K}} n^4 (V - E_K) - g_{\mathrm{L}}(V - E_{\mathrm{L}}) - I_w + I_{\mathrm{b}}, \\ \dot{h} &= \gamma\left[\alpha_h(V)(1-h) - \beta_h(V)h\right], \\ \dot{n} &= \gamma\left[\alpha_n(V)(1-n) - \beta_n(V)n\right], \\ \dot{w} &= a(1.5/(1+\exp((b-V)/k)) - w). \end{aligned} \tag{4}$$

Here, V is the transmembrane voltage, h and n are gating variables, w is used to determine the adaptation current I_w, and $I_{\mathrm{b}} = 5\mu\mathrm{A}/\mu\mathrm{F}$ is a baseline current chosen so that the neuron is in a periodically firing regime. A similar model was studied by [5] using the notion of a functional phase response curve, which gives a sense of an oscillator's asymptotic behavior in response to a specific periodic perturbation. Full model equations and parameters are given in Appendix B. For the choice of parameters used here, the neuron settles to a stable periodic orbit with natural period $T = 11.74$ ms.

The top panel of Figure 1 shows the isochrons calculated on a two-dimensional cross section for which $h = 0.234$ and $n = 0.305$. Here, we let $\theta = 0$ on the limit cycle correspond to the location where V crosses zero with positive slope (i.e., $(V, h, n, w) = (0, 0.234, 0.305, 0.052)$ for this choice of parameters). In experimental applications the asymptotic phase is usually difficult to measure and the timing of neural action potentials is generally of more practical interest (since the action potentials are related to the release of synaptic neurotransmitters). In this setting, the timing of an action potential might be defined as the time the variable V crosses a level set (such as $V = 0$), which we illustrate with a vertical dashed line in the top panel of Figure 1. Notice that the $\theta = 0$ level set does not directly correspond to a neural

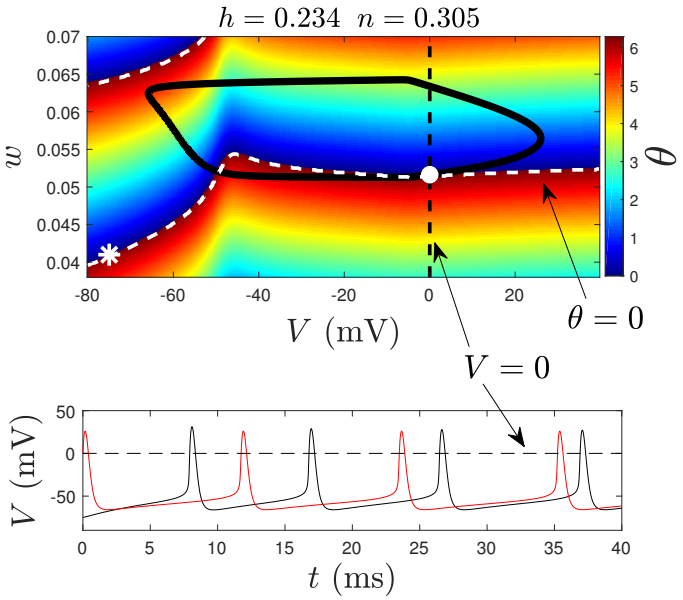

Figure 1. *The top panel shows the isochrons in a two-dimensional cross section of* (4) *for which* $h = 0.234$ *and* $n = 0.305$. *Isochrons are calculated according to* (3). *For reference, the periodic orbit is projected onto the* Vw*-plane (giving the illusion that isochrons intersect the periodic orbit multiple times) and is shown as a solid black line. The vertical dashed line corresponds to the* $V = 0$ *level set, i.e., a reasonable threshold that might be used to correspond to the timing of an action potential, and the curved dashed white line shows the* $\theta = 0$ *isochron. The white dot (resp., asterisk) shows an initial condition of* (4) *corresponding to the red (resp., black) voltage trace shown in the bottom panel obtained from direct numerical simulation. Even though both of these trajectories start on the* $\theta = 0$ *isochron, their transient behavior is different with spike times that do not align.*

spike and that this isochron is nearly perpendicular to the $V = 0$ threshold. The difference is particularly apparent when viewing the transmembrane voltage of two neurons with identical asymptotic phases in the bottom panel of Figure 1. While their behavior does converge in the limit as time approaches infinity, their transient behavior is different, with spikes occurring at different times. The qualitative mismatch between the $V = 0$ level set and the $\theta = 0$ isochron is a common feature of living neurons; when a neuron spikes the transmembrane voltage is rapidly changing and the phase generally has little sensitivity to perturbations to the transmembrane voltage (cf. [30]).

This discrepancy between the asymptotic definitions of phase and the measurable features of an experimental oscillator's state leads to many practical issues during implementation of phase reduction in living systems. For example, [28], [27] discuss the notion of a causality limit in measuring iPRCs in living neurons, whereby perturbations applied near the end of a cycle tend to elicit an immediate spike, limiting the measurement of an iPRC when large perturbations are applied. Additionally, various authors have investigated the effect of residual or higher order iPRCs [5], [30], [11], [31], [33], whereby perturbations can affect the timing of more than one subsequent action potential which alters phase locking predictions in some cases. These physiological behaviors represent a fundamental limitation of the phase reduction (2). While quantitative analysis is possible by measuring residual and higher order iPRCs [5],

[31], iPRCs must first be measured to analyze the effect of a specific type of perturbation, and no general framework exists for relating the iPRCs between different types of perturbations.

While phase reduction (2) is particularly useful for investigating the steady state behavior of a perturbed oscillator, it is often inadequate to predict its transient behavior. As such, when oscillators are subject to recurrent, aperiodic perturbations, or when perturbations decay slowly back to the limit cycle, (2) may not adequately capture the behavior of the full system (1). In this work, we propose an operational phase defined to have a direct correspondence to the moment a given variable crosses a specific threshold Poincaré section [42], such as the $V = 0$ threshold shown in Figure 1. As we will show, the resulting operational phase reduction (OPR) correctly predicts both the asymptotic and transient behavior of a perturbed oscillator. Furthermore, the relatively simple definition of phase in this context makes it applicable when data with high temporal resolution is limited, e.g., in neurons where transmembrane voltage is typically the most readily available measurement. The organization of this paper is as follows: section 2 investigates the theoretical details required to define the OPR, and section 3 investigates a direct method for calculation for all required terms in the OPR. Section 4 gives examples illustrating the contrast between asymptotic and OPRs, and section 5 gives concluding remarks.

2. Operational phase coordinates and reduction. The goal of this section is to develop a reduced coordinate system $\theta^*(x) \in [0, 2\pi)$ such that $\theta^*(x) = 0$ corresponds to the moment at which an arbitrarily chosen variable crosses an arbitrarily chosen threshold near the limit cycle. We will refer to these as operational phase coordinates because $\theta^* = 0$ corresponds to some feature of the system that is directly measurable and may be of interest on every cycle. For example, we might define $\theta^* = 0$ as the time that a periodically spiking neuron fires an action potential and elevates its voltage beyond its resting level. Intuitively, this threshold defines a Poincaré section [42], and the time required for the operational phase to start at and return to $\theta^* = 0$ corresponds to the return time to this Poincaré section. By contrast, the asymptotic phase, θ, of a neuron can only be directly measured once the state returns sufficiently close to the limit cycle.

We will define the operational phase using the isostable coordinates described in [44]. These isostable coordinates, ψ_i for $i = 1, \ldots, N-1$, give a sense of the distance in a particular direction transverse to the periodic orbit. In the absence of external perturbations, isostable coordinates decay exponentially, making them useful in many practical applications. Other strategies for obtaining phase-amplitude coordinate systems have also been proposed (cf. [4], [41], [36]) and are useful in other contexts.

We will also analyze operational phase in a reduced coordinate framework and derive formal relationships between the previously established augmented phase reduction from [44], [46]. The augmented isostable reduction given below tracks how both the asymptotic phase and isostable coordinates change over time in response to small perturbations provided the state remains close to the limit cycle. Such a coordinate transformation allows (1) to be represented by

$$\begin{aligned} \dot{\theta} &= \omega + \mathcal{Z}(\theta)^T G(t), \\ \dot{\psi}_i &= \kappa_i \psi_i + \mathcal{I}_i(\theta)^T G(t), \\ & \qquad i = 1, \ldots, N-1. \end{aligned} \tag{5}$$

Here, κ_i is the Floquet exponent corresponding to the isostable coordinate ψ_i, $\mathcal{I}_i$ is the infinitesimal isostable response curve (iIRC) associated with the ith isostable coordinate, and all other terms are defined identically to those in (2). It is generally assumed that $G(t)$ is of order ϵ where $0 < \epsilon \ll 1$ and that $\epsilon \ll |\kappa_i|$ for all i so that ψ_i is also an order ϵ term. More technical details about (5) based on analysis from [44] and [46] are given in Appendix A. Provided some isostable coordinates of (5) decay rapidly, i.e., with $|\kappa_i|$ being large relative to the magnitude of $G(t)$, these coordinates can be approximated to be zero and neglected.

2.1. Defining operational phase. From this point on, we will refer to a reduction of the form (5) as an asymptotic phase reduction (APR). Our operational phase coordinate, $\theta^*(x)$, is a function of the state x and will be related to the phase and isostable coordinates from (5). We will use two definitions which reflect the original motivation for developing the notion of operational phase coordinates.

Definition 1 ($\theta^* = 0$ level set). *Let γ be a stable limit cycle. Let $x^\gamma(0)$ correspond to $x \in \gamma$ for which $\theta(x) = 0$. Choose $k \in \mathbb{N} \leq n$, and let $x_k^\gamma(0)$ and x_k be the kth element of $x^\gamma(0)$ and x, respectively. The $\theta^*(x) = 0$ level set is defined to be all states x in some neighborhood of $x^\gamma(0)$ for which $x_k = x_k^\gamma(0)$ and $\text{sign}(|\frac{dx_k}{dt}|_x) = \text{sign}(\frac{dx_k}{dt}|_{x^\gamma(0)})$.*

Definition 2 (time derivative of θ^*). *In the basin of attraction of the limit cycle, phase coordinates evolve according to*

$$\dot{\theta}^* = \omega + d(\psi_1, \ldots, \psi_{N-1}) + \frac{\partial \theta^*}{\partial x}^T \Big|_{x(t)} G(t), \tag{6}$$

where $\theta^*(x) \in [0, 2\pi)$, d is a function of the isostable coordinates that is generally not known a priori and must be chosen such that Definitions 1 and 2 do not contradict each other (more about the function d will be discussed below), and the gradient with respect to x is used to capture the effects of infinitesimal perturbations on the operational phase. In (6), explicit dependence of the variables θ^*, θ, ψ_1, ..., and ψ_N on x has been dropped for notational convenience. Using Definitions 1 and 2, one can show by contradiction that $d(0, \ldots, 0) = 0$. Thus, on the limit cycle, the unperturbed dynamics of both θ and θ^* increase at a constant rate ω so that $\theta^*(x) = \theta(x)$ for every $x \in \gamma$.

Definition 1 reflects the original motivation of developing operational phase coordinates, that is, to use a coordinate system for which the $\theta^* = 0$ level set corresponds to the moment an arbitrary variable crosses some prescribed threshold. Note that this $\theta^* = 0$ level set could be used to define a Poincaré section. Definition 2 states that the time derivative of the operational phase is a function of the isostable coordinates and will be used to extend the notion of operational phase to the basin of attraction of the limit cycle. The dynamics of θ^* could be chosen differently, but as we will see, our choice will allow for the derivation of relationships between the asymptotic and operational phase coordinates which makes the comparison between these coordinates systems tractable. Also, unlike when using asymptotic phase coordinates, two separate initial conditions with the same operational phase coordinate will not necessarily share the same convergence to the periodic orbit.

By setting $G = 0$, for any initial condition in the basin of attraction of γ the operational and asymptotic phases converge as time approaches infinity. Recalling that $\dot{\theta} = \omega$ when $G = 0$

and that $\dot{\theta}^*$ is given by (6), integrating $\frac{d}{dt}(\theta^*(t)-\theta(t))$ in the limit as time approaches infinity yields

$$\theta^*(0) = \theta(0) - \int_0^\infty d(\psi_1, \ldots, \psi_{N-1})dt. \tag{7}$$

The relationship prescribed by the function d in (7) must be consistent with the definition of the $\theta^* = 0$ level set. In general, this fully nonlinear function d is difficult to find explicitly. However, as we will show in the examples to follow, it can be useful to approximate it by Taylor expanding, assuming that all isostable coordinates are $\mathcal{O}(\epsilon)$, to yield

$$d(\psi_1, \psi_2, \ldots, \psi_{N-1}) = \sum_{j=1}^{N-1} (\alpha_j \psi_j) + \sum_{j=1}^{N-1} \sum_{k=1}^{j} (\beta_{k,j} \psi_k \psi_j) + \mathcal{O}(\epsilon^3). \tag{8}$$

Here, the terms α_j and $\beta_{k,j}$ represent the constant terms of the Taylor expansion. As noted in Appendix A, in the absence of perturbations, isostable coordinates decay exponentially so that $\psi_i(t) = \psi_i(0)\exp(\kappa_i t)$. This feature, along with (7), implies the following relation for a given initial condition which is accurate to $\mathcal{O}(\epsilon^2)$:

$$\begin{aligned} \theta(0) &= \theta^*(0) + \int_0^\infty \sum_{j=1}^{N-1} \left(\alpha_j \psi_j(t) + \sum_{k=1}^{j} (\beta_{k,j} \psi_k(t) \psi_j(t)) \right) dt \\ &= \theta^*(0) - \sum_{j=1}^{N-1} \left(\frac{\alpha_j \psi_j(0)}{\kappa_j} + \sum_{k=1}^{j} \left(\frac{\beta_{k,j} \psi_k(0) \psi_j(0)}{\kappa_k + \kappa_j} \right) \right). \end{aligned} \tag{9}$$

Equation (9) is valid for any initial conditions close enough to the periodic orbit which gives us a direct relationship between the operational and asymptotic phase at any time,

$$\theta = \theta^* - \sum_{j=1}^{N-1} \left(\frac{\alpha_j \psi_j}{\kappa_j} + \sum_{k=1}^{j} \left(\frac{\beta_{k,j} \psi_k \psi_j}{\kappa_k + \kappa_j} \right) \right). \tag{10}$$

In the sections to follow, we will use the above relation to investigate an OPR in relation to the APR (5).

2.2. First order operational phase reduction. Equation (5) is a first order approximation of the asymptotic phase dynamics which assumes that $G(t) = \mathcal{O}(\epsilon)$ and that the trajectory remains close to the limit cycle (i.e., that $\psi_i = \mathcal{O}(\epsilon)$ for all i). By making similar assumptions, starting with (6) and retaining terms up to and including $\mathcal{O}(\epsilon)$, we arrive at a first order accurate OPR:

$$\begin{aligned} \dot{\theta}^* &= \omega + \sum_{j=1}^{N-1} (\alpha_j \psi_j) + \mathcal{Z}^*(\theta^*)^T \, G(t), \\ \dot{\psi}_i &= \kappa_i \psi_i + \mathcal{I}_i^*(\theta^*)^T G(t), \\ & \qquad i = 1, \ldots, N-1. \end{aligned} \tag{11}$$

Notice the similarity between the above definition and the augmented phase reduction (5). Here, isostable coordinates ψ_i are identical to those from the augmented phase reduction, functions $\mathcal{Z}^*(\theta^*) \equiv \frac{\partial \theta^*}{\partial x}|_{x^\gamma(\theta^*)}$, and $\mathcal{I}_i^*(\theta^*) \equiv \frac{\partial \psi_i}{\partial x}|_{x^\gamma(\theta^*)}$ with $x^\gamma(\theta^*)$ defined to be the intersection of the periodic orbit and the θ^* level set. Here, the functions $\mathcal{Z}^*$ and $\mathcal{I}_i^*$ are analogous to $\mathcal{Z}$ and $\mathcal{I}_i$, and each α_i provides an $\mathcal{O}(\epsilon)$ correction to the natural frequency for locations away from the limit cycle. To derive a relationship between the APR and OPR, we can substitute (10) into (5), keeping only $\mathcal{O}(\epsilon)$ terms to yield

$$\begin{aligned}\dot{\theta}^* - \sum_{j=1}^{N}\left(\frac{\alpha_j \dot{\psi}_j}{\kappa_j}\right) &= \omega + \mathcal{Z}\left(\theta^* - \sum_{j=1}^{N}\left(\frac{\alpha_j \psi_j}{\kappa_j}\right)\right)^T G(t),\\ \dot{\psi}_i &= \kappa_i \psi_i + \mathcal{I}_i\left(\theta^* - \sum_{j=1}^{N}\left(\frac{\alpha_j \psi_j}{\kappa_j}\right)\right)^T G(t).\end{aligned} \tag{12}$$

Taylor expanding (12) and appropriately collecting all $\mathcal{O}(\epsilon)$ terms allows us to write (12) in the form (11) with the following relationship between the terms of the APR and OPR:

$$\begin{aligned}\mathcal{I}_i^*(\theta^*) &= \mathcal{I}_i(\theta^*),\\ \mathcal{Z}^*(\theta^*) &= \mathcal{Z}(\theta^*) + \sum_{j=1}^{N}\left(\frac{\alpha_j \mathcal{I}_j(\theta^*)}{\kappa_j}\right).\end{aligned} \tag{13}$$

Thus, if the APR is known, all functions in the OPR can be calculated with knowledge of the constants α_j. Toward the determination of an arbitrarily chosen α_j, consider the periodic orbit and a solution of the full system (1) for which $\theta(t_0) = 0$, $\psi_j(t_0) = \mathcal{O}(\epsilon)$, and $\psi_i(t_0) = 0$ for all $i \neq j$. Assume also that $G(t) = 0$ when $t > t_0$. From (51) in Appendix A the initial state is given to leading order ϵ by

$$x(t_0) = x^\gamma(0) + \psi_j p_j(0), \tag{14}$$

where $x^\gamma(\theta)$ represents the location on the periodic orbit as a function of θ and $p_j(\theta)$ relates the isostable coordinate to a perturbation from the limit cycle. Figure 2 illustrates the relationship between the operational and asymptotic phase coordinates for a planar system. As a function of t_0, a given trajectory will cross the $\theta^* = 0$ level set at time t_0^* given to leading order as

$$t_0^* = t_0 - \frac{\psi_j(t_0) p_j^{x_k}(0)}{\dot{x}_k(0)} + \mathcal{O}(\epsilon^2), \tag{15}$$

where $p_j^{x_k}(\theta)$, and $\dot{x}_k(\theta)$ are the components of $p_j(\theta)$ and $\dot{x}(\theta)$, respectively, in the x_k direction. Both of these functions are evaluated on the periodic orbit. Intuitively, (15) states that the difference in the times t_0 and t_0^* is equal to the distance between the $\theta^* = 0$ and $\theta = 0$ level set divided by the "speed" on γ, both taken in the x_k direction. As a brief aside, for a dynamical system which does not receive any inputs, (15) could be used in conjunction with (5) to obviate the need for operational phase coordinates, as t_0^* can be determined to leading order ϵ by simply knowing t_0 and the corresponding isostable coordinates. However, when perturbations are allowed (15) alone would not be enough to determine t_0^*.

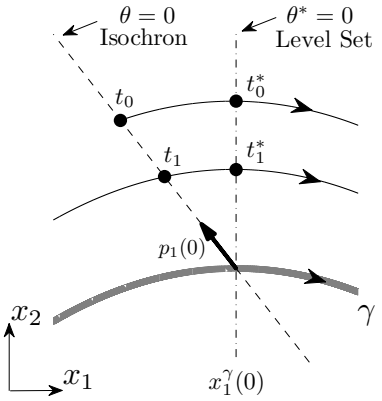

Figure 2. *A planar system schematic of the $\theta = 0$ isochron (diagonal dashed line), defined by the asymptotic approach to the periodic orbit and $\theta^* = 0$ level set (vertical dashed line) defined by the crossing of the threshold $x_1^\gamma(0)$. The gray line represents the periodic orbit and the black line represents a trajectory for which $\theta(t_0) = 0$, $\psi_1(t_0) \neq 0$, and $G(t) = 0$ for $t > t_0$. At locations close enough to the limit cycle, $\psi_1 p_1(\theta)$ determines the deviation from the limit cycle; $p_1(0)$ is tangent to the $\theta = 0$ level set. By relating the times between crossings of the $\theta = 0$ and $\theta^* = 0$ level sets, one can numerically determine the coefficient α_j according to (18).*

When $G(t) = 0$ subsequent crossings of the $\theta = 0$ level set will occur at $t_n = t_0 + nT$. Therefore, at these crossings, the associated isostable coordinate is $\psi_j(t_0 + nT) = \lambda_j^n \psi_j(t_0)$, where λ_j is the jth Floquet multiplier. Therefore, using the same reasoning used to obtain t_0^*,

$$t_n^* = t_0 + nT - \frac{\psi_j(t_0)\lambda_j^n p_j^{x_k}(0)}{\dot{x}_k(0)} + \mathcal{O}(\epsilon^2). \tag{16}$$

Finally, integrating (11) forward in time from t_0^* to t_1^* and dropping the $\mathcal{O}(\epsilon^2)$ terms we have

$$\begin{aligned}
\int_{t_0^*}^{t_1^*} (\omega + \alpha_j \psi_j)\, dt &= 2\pi, \\
\frac{\alpha_j \psi_j(t_0)}{\kappa_j} \left(\exp(\kappa_j(t_1^* - t_0)) - \exp(\kappa_j(t_0^* - t_0))\right) &= 2\pi - \omega(t_1^* - t_0^*), \\
\frac{\alpha_j \psi_j(t_0)}{\kappa_j} \left(\exp(\kappa_j(t_1^* - t_0)) - \exp(\kappa_j(t_0^* - t_0))\right) &= \frac{\psi_j(t_0)\omega(\lambda_j - 1)p_j^{x_k}(0)}{\dot{x}_k(0)}.
\end{aligned} \tag{17}$$

In the above equation, the second line is obtained by noting that $\psi_j(t) = \psi_j(t_0)\exp(\kappa_j(t - t_0))$ in the integral, and the third line is obtained by using (15) and (16) to substitute $t_1^* - t_0^*$ and simplify recalling $2\pi = \omega T$. Continuing to simplify (17),

$$\begin{aligned}
\frac{\alpha_j \psi_j(t_0)}{\kappa_j} \left(\lambda_j \exp(\lambda_j \kappa_j(t_0^* - t_0)) - \exp(\kappa_j(t_0^* - t_0))\right) &= \frac{\psi_j(t_0)\omega(\lambda_j - 1)p_j^{x_k}(0)}{\dot{x}_k(0)}, \\
\alpha_j &= \frac{\omega \kappa_j p_j^{x_k}(0)}{\dot{x}_k(0)}.
\end{aligned} \tag{18}$$

The first line of (18) is obtained from (17) by using the relation $t_1^* - t_0 = T + \lambda_j(t_0^* - t_0)$, and the last line is obtained through algebraic manipulation after noting that $\lambda_j \exp(\lambda_j \kappa_j(t_0^* -$

$t_0)) - \exp(\kappa_j(t_0^* - t_0)) = \lambda_j - 1 + \mathcal{O}(t_0^* - t_0)$ and recalling that $(t_0^* - t_0)$ and $\psi_j(t_0)$ are both $\mathcal{O}(\epsilon)$ terms. Equation (18) can be used to find α_j corresponding to the isostable coordinate ψ_j.

2.3. Second order operational phase reduction. In [44] a strategy is developed for increasing the accuracy of standard phase reduction (2) when the state is far from the periodic orbit. The resulting equations are similar to the APR from (5), with additional correction terms

$$\begin{aligned}
\dot{\theta} &= \omega + \left[\mathcal{Z}(\theta)^T + \sum_{j=1}^{N-1} \left(\psi_j \mathcal{B}_j(\theta)^T\right)\right] G(t),\\
\dot{\psi}_i &= \kappa_i \psi_i + \left[\mathcal{I}_i(\theta)^T + \sum_{j=1}^{N-1} \left(\psi_j \mathcal{D}_j^i(\theta)^T\right)\right] G(t),\\
& \qquad i = 1, \ldots, N-1.
\end{aligned} \tag{19}$$

Here, the functions $B_j(\theta)$ and $D_j^i(\theta)$ provide a correction to the gradient of the isostable and phase coordinates for each ψ_i, and the remaining terms are identical to those presented in the first order accurate reduction (5). A brief description of the terms in the reduction (19) is given in Appendix A, with a more in-depth explanation given in [44]. Similar to the results in the previous section, we can define a second order accurate OPR by retaining all terms up to and including order $\mathcal{O}(\epsilon^2)$ in the Taylor expansion of (6)

$$\begin{aligned}
\dot{\theta}^* &= \omega + \sum_{j=1}^{N-1} (\alpha_j \psi_j) + \sum_{j=1}^{N-1} \sum_{k=1}^{j} (\beta_{k,j} \psi_k \psi_j) + \left[\mathcal{Z}^*(\theta^*)^T + \sum_{j=1}^{N-1} \left(\psi_j \mathcal{B}_j^*(\theta^*)^T\right)\right] G(t),\\
\dot{\psi}_i &= \kappa_i \psi_i + \left[\mathcal{I}_i^*(\theta^*)^T + \sum_{j=1}^{N-1} \left(\psi_j \mathcal{D}_j^{i*}(\theta^*)^T\right)\right] G(t),\\
& \qquad i = 1, \ldots, N-1.
\end{aligned} \tag{20}$$

Here, the terms $\mathcal{B}_j^*$ and $\mathcal{D}_j^{i*}$ are analogous to the terms $\mathcal{B}_j$ and $\mathcal{D}_j^i$ from (19), the terms $\beta_{k,j}$ give a second order correction to the natural frequency for locations away from the limit cycle, and the remaining terms are identical to those presented in the first order accurate reduction (11). Note that in (20), the number of terms $\beta_{k,j}$ in the second order accurate reduction (20) increase at a rate proportional to N^2, and it is generally difficult to obtain all of these constants. In this section, we will focus on the case where all but one isostable coordinate rapidly decays, i.e., $|\kappa_i|$ is large for all $i \geq 2$ so that the isostable coordinates $\psi_2, \ldots, \psi_{N-1}$ are well approximated by zero (cf. [46], [44]). With this assumption, it is clear from (20) that we can also ignore $\beta_{k,j}$ for $k \geq 2$ or $j \geq 2$. Using a strategy similar to that of the previous section, we substitute terms from (10) into (19), Taylor expand assuming ψ_1 is an $\mathcal{O}(\epsilon)$ term, and retain all $\mathcal{O}(\epsilon^2)$ terms to obtain the functions $\mathcal{B}_1^*(\theta^*)$ and $\mathcal{D}_1^{1*}$ in relation to the functions

from (19),

$$\mathcal{D}_1^{1*}(\theta^*) = \mathcal{D}_1^1(\theta^*) - \frac{\alpha_1}{\kappa_1}\mathcal{I}_1'(\theta^*),$$
$$\mathcal{B}_1^*(\theta^*) = \mathcal{B}_1(\theta^*) + \frac{\beta_{1,1}}{\kappa_1}\mathcal{I}_1(\theta^*) - \frac{\alpha_1}{\kappa_1}\left(\mathcal{Z}'(\theta^*) - \mathcal{D}_1^1(\theta^*) + \frac{\alpha_1}{\kappa_1}\mathcal{I}'(\theta^*)\right), \tag{21}$$

where $' \equiv d/d\theta^*$. Equation (18) is still valid for calculating α_1, so that only the additional calculation of $\beta_{1,1}$ is required to evaluate the terms in (21).

For planar systems (i.e., with $N = 2$), a relatively simple equation can be derived to obtain $\beta_{1,1}$ in relation to the terms in the APR. To begin, consider any initial condition $x \in \gamma$ corresponding to an asymptotic phase θ (recall that $\theta = \theta^*$ on γ) and an $\mathcal{O}(\epsilon)$ perturbation $x_\epsilon = x + \Delta x$. The change in asymptotic phase, operational phase, and isostable coordinates caused by this perturbation can be approximated to leading order ϵ^2 by $\theta(x_\epsilon) = \theta + \mathcal{Z}(\theta)^T\Delta x + \Delta x^T\mathcal{H}_\theta(\theta)\Delta x$, $\theta^*(x_\epsilon) = \theta^* + \mathcal{Z}^*(\theta)^T\Delta x + \Delta x^T\mathcal{H}_{\theta^*}(\theta)\Delta x$, and $\psi_1(x_\epsilon) = \mathcal{I}(\theta)^T\Delta x + \Delta x^T\mathcal{H}_{\psi_1}(\theta)\Delta x$. Here $\mathcal{H}_A(\theta)$ is the Hessian matrix of second partial derivatives of the coordinate $A \equiv \theta$, θ^* and ψ_1 evaluated at $x^\gamma(\theta)$. Substituting the above relations into (10) when $N = 2$ and collecting $\mathcal{O}(\epsilon^2)$ terms yields the following:

$$\frac{1}{2}\Delta x^T\mathcal{H}_\theta(\theta)\Delta x = \frac{1}{2}\Delta x^T\mathcal{H}_{\theta^*}(\theta)\Delta x - \frac{1}{2}\Delta x^T\frac{\alpha_1}{\kappa_1}\mathcal{H}_{\psi_1}(\theta)\Delta x - \frac{\beta_{1,1}}{2\kappa_1}\Delta x^T\mathcal{I}_1(\theta)\mathcal{I}_1^T(\theta)\Delta x. \tag{22}$$

The equation above is valid for arbitrary perturbations Δx so that

$$\mathcal{H}_\theta(\theta) = \mathcal{H}_{\theta^*}(\theta) - \frac{\alpha_1}{\kappa_1}\mathcal{H}_{\psi_1}(\theta) - \frac{\beta_{1,1}}{\kappa_1}\mathcal{I}_1(\theta)\mathcal{I}_1(\theta)^T. \tag{23}$$

Recall that the operational phase is defined so that $\theta^* = 0$ when x_k crosses the threshold $x_k^\gamma(0)$. For a planar system we will without loss of generality take $k = 1$. This definition implies that $\frac{\partial^2\theta^*}{\partial x_2^2} = 0$ whenever $\theta^* = 0$ because perturbations that do not change the x_1 coordinate at $\theta^* = 0$ remain on the $\theta^* = 0$ level set. Therefore, $e_2^T\mathcal{H}_{\theta^*}(0)e_2 = 0$ where $e_2 = [0\ 1]^T$ and by multiplying each term of (23) on the left and right by e_2^T and e_2, respectively, and simplifying we have

$$\begin{aligned}\beta_{1,1} &= \frac{e_2^T\kappa_1\mathcal{H}_\theta(0)e_2 + e_2^T\alpha_1\mathcal{H}_{\psi_1}(0)e_2}{-e_2^T\mathcal{I}_1(0)\mathcal{I}_1^T(0)e_2} \\ &= -\left[\kappa_1\frac{\partial^2\theta}{\partial x_2^2} + \alpha_1\frac{\partial^2\psi_1}{\partial x_2^2}\right] \Big/ \left(\frac{\partial\psi_1}{\partial x_2}\right)^2,\end{aligned} \tag{24}$$

where all partial derivatives are evaluated at $\theta = 0$ on the limit cycle.

To summarize, all terms of the second order accurate OPR (20) can be determined if the second order APR (19) has already been calculated for planar systems. Specifically, $\beta_{1,1}$ and α_1 can be calculated using (24) and (18), respectively. The remaining functions are supplied by the relations (21) and (13). In higher dimensions the calculation of each $\beta_{k,j}$ becomes more complicated and is not discussed here. In special situations where $N > 2$ and all but one isostable coordinate decays rapidly, the reduction (21) only requires knowledge of $\beta_{1,1}$ and it may be more efficient to estimate this term using a fit to numerical data.

2.4. nth order iPRCs in relation to operational phase reduction. The standard phase reduction (2) assumes that perturbations to the full system (1) decay rapidly to the periodic orbit [47], justifying its study on a one-dimensional manifold. In practice, however, this assumption is not always true. For instance, in neurons it is well documented that a perturbation during a given cycle can influence not only the timing of the next spike but also the timing of subsequent spikes [32], [29]. This phenomenon is often referred to as higher order resetting, from which nth order iPRCs can be measured [5], [24], [31]. For small perturbations from the limit cycle, the sum of all nth order iPRCs yields the asymptotic iPRC, $\mathcal{Z}(\theta)$. The effect of larger periodic perturbations can also be investigated, yielding a functional phase response curve [5], [37] which can be used to study the asymptotic behavior of systems resulting from specific periodic perturbations.

While higher order iPRCs have been used to investigate neural behavior, their relationship to the underlying system dynamics is not well understood. Here, using the first order accurate version of the OPR (11), we show that, provided perturbations from the limit cycle are small enough, all higher order phase response curves are exponentially decaying functions of the isostable response curves. To begin, consider an initial condition on the limit cycle which yields a spike at $t = t_0$. If we apply a small perturbation Δx at t_p, where $t_0 \le t_p \le (T + t_0)$, the phase at which the perturbation is applied is $\theta_p^* = \omega(t_p - t_0)$. Letting $G \equiv 0$ at all other times, the the timing of the nth spike occurring at t_n solves the equation

$$\begin{aligned} 2\pi n &= \int_{t_0}^{t_p} \omega dt + \mathcal{Z}^*(\theta_p^*)^T \Delta x + \int_{t_p}^{t_n} \left(\omega + \sum_{j=1}^{N-1} \alpha_j \psi_j(t)\right) dt \\ &= \theta_p^* + \omega(t_n - t_p) + \mathcal{Z}^*(\theta_p^*)^T \Delta x + \sum_{j=1}^{N-1} \frac{\alpha_j \mathcal{I}_j^*(\theta_p^*)^T \Delta x}{\kappa_j} \left(\exp(\kappa_j(t_n - t_p)) - 1\right). \end{aligned} \tag{25}$$

Using (25), one can show with algebraic manipulation that the residual effects on the interspike interval (ISI) which yield higher order iPRCs are given by

$$t_n - t_{n-1} = T - \sum_{j=1}^{N-1} \frac{\alpha_j \mathcal{I}_j^*(\theta_p^*)^T \Delta x}{\omega \kappa_j} \left(\exp(\kappa_j(t_n - t_p)) - \exp(\kappa_j(t_{n-1} - t_p))\right). \tag{26}$$

Equation (26) states that the nth ISI is equal to the natural period plus the sum of $N - 1$ exponentially decaying functions which are proportional to the iIRC.

2.5. Asymptotic behavior for weak periodic perturbations. Here we consider the infinite time behavior of the OPR (11) and the APR (5) for a general limit cycle oscillator in the weakly perturbed limit. Consider the infinite time behavior of (1) when $G(t)$ is an $\mathcal{O}(\epsilon)$, T_p-periodic perturbation. Furthermore, suppose $\omega_p = 2\pi/T_p$ is within $\mathcal{O}(\epsilon)$ of the natural frequency ω of the limit cycle oscillator. Starting with operational phase coordinates, we change variables to a rotating reference frame $\phi^* = \theta^* - \omega_p t$ so that the first order OPR (11) can be written as

$$\begin{aligned} \dot{\phi}^* &= (\omega - \omega_p) + \sum_{j=1}^{N-1} (\alpha_j \psi_j) + \mathcal{Z}^*(\phi^* + \omega_p t)^T G(t) + \mathcal{O}(\epsilon^2), \\ \dot{\psi}_i &= \kappa_i \psi_i + \mathcal{I}_i^*(\phi^* + \omega_p t)^T G(t) + \mathcal{O}(\epsilon^2), \quad i = 1, \ldots, N-1. \end{aligned} \tag{27}$$

Notice that the above equation is T_p-periodic. We assume that $|\kappa_i|$ are large relative to ϵ and that the dynamics remain close enough to the periodic orbit so that ψ_i are $\mathcal{O}(\epsilon)$ terms. This allows us to use formal averaging techniques [35], [15] to approximate (27) as

$$\begin{aligned}\dot{\Phi}^* &= P(\Phi^*) + \sum_{j=1}^{N-1}(\alpha_j \Psi_j),\\ \dot{\Psi}_i &= \kappa_i \Psi_i + Q_i(\Phi^*), \quad i = 1,\dots,N-1.\end{aligned} \tag{28}$$

Here $P(\Phi^*) = \frac{1}{T_p}\int_0^{T_p}[\omega - \omega_p + \mathcal{Z}^*(\Phi^* + \omega_p t)^T G(t)]dt$, $Q_i(\Phi^*) = \frac{1}{T_p}\int_0^{T_p}[\mathcal{I}_i^*(\Phi^* + \omega_p t)^T G(t)]dt$, and Φ^* and Ψ_i are close approximations to ϕ^* and ψ_i.

We also consider the APR of (1). Here we will neglect the isostable dynamics and focus on the dynamics of the phase coordinate, i.e., $\dot{\theta} = \omega + \mathcal{Z}(\theta)^T G(t)$. The change of variables $\phi = \theta - \omega_p t$ yields

$$\dot{\phi} = (\omega - \omega_p) + \mathcal{Z}(\phi + \omega_p t)^T G(t) + \mathcal{O}(\epsilon^2). \tag{29}$$

Similar to (27), the above equation can be averaged in the weak forcing limit to yield the approximation

$$\dot{\Phi} = R(\Phi), \tag{30}$$

where $R(\Phi) = \frac{1}{T_p}\int_0^{T_p}[\omega - \omega_p + \mathcal{Z}(\Phi + \omega_p t)^T G(t)]dt$, and Φ is a close approximation to ϕ. In this example, averaging is particularly useful to analyze the infinite time behavior of each reduced system, because fixed points of (28) (resp., (30)) correspond to periodic orbits of (27) (resp., (29)) with the same stability [35].

In the analysis to follow, we will show that if (28) has a fixed point at Φ^*_{fp}, then (30) also has a fixed point at $\Phi_{\text{fp}} = \Phi^*_{\text{fp}}$ with the same stability. We will also show that the converse is true, i.e., that if (30) has a fixed point, (28) has the same fixed point with identical stability. Here, the following relation between P, Q, and R will be particularly useful:

$$\begin{aligned}R(\Phi) &= \frac{1}{T_p}\int_0^{T_p}[\omega - \omega_p + \mathcal{Z}(\Phi + \omega_p t)^T G(t)]dt\\ &= \frac{1}{T_p}\int_0^{T_p}\left[\omega - \omega_p + \left(\mathcal{Z}^*(\Phi + \omega_p t) - \sum_{j=1}^{N-1}\left(\frac{\alpha_j \mathcal{I}(\Phi + \omega_p t)}{\kappa_j}\right)\right)^T G(t)\right]dt\\ &= P(\Phi) - \sum_{j=1}^{N-1}\left(\frac{\alpha_j Q_j(\Phi)}{\kappa_j}\right),\end{aligned} \tag{31}$$

where the first line is true by definition, and the second line is obtained using (13). Keeping (31) in mind, suppose (28) has a fixed point at

$$\begin{bmatrix}\Phi^* & \Psi_1 & \dots & \Psi_{N-1}\end{bmatrix}^T = \begin{bmatrix}\Phi^*_{\text{fp}} & \Psi_{1,\text{fp}} & \dots & \Psi_{N-1,\text{fp}}\end{bmatrix}^T.$$

This can be true only when $\Psi_{i,\text{fp}} = -Q_i(\Phi^*_{\text{fp}})/\kappa_i$ for all i, and it follows from the top equation in (28) that $P(\Phi^*_{\text{fp}}) - \sum_{j=1}^{N-1}(\frac{\alpha_j}{\kappa_i}Q_j(\Phi^*_{\text{fp}})) = 0$. Noting the relation in (31), this implies that $R(\Phi^*) = 0$, and in the weakly perturbed limit, fixed points of (28) and (30) are identical.

The stability of a fixed point of (30) can be determined simply by considering the sign of $dR/d\Phi$ evaluated at the fixed point. Determining the stability of a fixed point of (28) is more difficult and is dependent on the eigenvalues of the Jacobian, J, of (28) evaluated at the fixed point where

$$J = A + E,$$

$$A \equiv \begin{bmatrix} 0 & \alpha_1 & \alpha_2 & \dots & \alpha_{N-1} \\ 0 & \kappa_1 & 0 & \dots & 0 \\ 0 & 0 & \kappa_2 & & \vdots \\ \vdots & \vdots & & \ddots & 0 \\ 0 & 0 & \dots & 0 & \kappa_{N-1} \end{bmatrix}, \quad E \equiv \begin{bmatrix} P'(\Phi^*_{\rm fp}) & 0 & \dots & 0 \\ Q_1'(\Phi^*_{\rm fp}) & 0 & \dots & 0 \\ \vdots & \vdots & & \vdots \\ Q'_{N-1}(\Phi^*_{\rm fp}) & 0 & \dots & 0 \end{bmatrix}. \tag{32}$$

Here, the Jacobian of (28) is split into the matrix A, which contains $\mathcal{O}(1)$ terms, and the matrix E, which contains $\mathcal{O}(\epsilon)$ terms, and $' \equiv \partial/\partial\Phi^*$. Note that all terms in (32) are real-valued. Toward determining the eigenvalues of J, we will consider the eigenvalues λ_i of A in response the effect of the $\mathcal{O}(\epsilon)$ perturbation, E. In the unperturbed case, the eigenvalues can be read off the diagonal, with $\lambda_1 = 0$ and $\lambda_i = \kappa_{i-1}$ for $i = 2, \dots, N$. Suppose for the moment each κ_i is unique so that all eigenvalues are simple (i.e., with algebraic multiplicity equal to 1). Then, as shown in section 4.3 of [6], to leading order ϵ, the eigenvalues of $A + E$ are given by

$$\tilde{\lambda}_i = \lambda_i + u_i^* E v_i/(u_i^* v_i), \tag{33}$$

where u_i^* and v_i are the left and right eigenvectors of A corresponding to λ_i. Additionally, since A and its eigenvalues are real-valued, its left and right eigenvalues must also be real-valued so that to leading order ϵ, $\tilde{\lambda}_i$ remain real-valued. Note that all κ_i are negative because the limit cycle is stable. Therefore, for ϵ small enough, $\tilde{\lambda}_i$ remains negative for $i = 2, \dots, N$. If some of the values κ_i are not unique, we can still guarantee that $\tilde{\lambda}_i < 0$ for $i \geq 2$ and when ϵ is small enough, but the expansion may include fractional powers of ϵ (cf. Chapter 2 of [20]). The sign of the remaining eigenvalue can be determined by noting that the left and right eigenvalues of $\lambda_1 = 0$ are $[1 \ \frac{-\alpha_1}{\kappa_1} \ \dots \ \frac{-\alpha_{N-1}}{\kappa_{N-1}}]$ and $[1 \ 0 \ \dots \ 0]^T$, respectively. According to (33),

$$\begin{aligned} \tilde{\lambda}_1 &= P'(\Phi^*_{\rm fp}) - \sum_{k=1}^{N-1} \left(\frac{\alpha_k Q_k'(\Phi^*_{\rm fp})}{\kappa_k} \right) + \mathcal{O}(\epsilon^2) \\ &= R'(\Phi^*_{\rm fp}) + \mathcal{O}(\epsilon^2). \end{aligned} \tag{34}$$

Equation (34) implies that the stability of corresponding fixed points of (28) and (30) is the same.

Toward showing that if (30) has a fixed point, (28) has the same fixed point with identical stability, suppose $R(\Phi_{\rm fp}) = 0$ for some value of $\Phi_{\rm fp}$. Using the operational phase reduced framework from (28), for $i = 1, \dots, N-1$, we can find $\Psi_{i,\rm fp}$ such that $\kappa_i \Psi_{i,\rm fp} + Q_i(\Phi_{\rm fp}) = 0$. Manipulation yields $\Psi_{i,\rm fp} = -Q_i(\Phi_{\rm fp})/\kappa_i$. Substituting this relation into the right-hand side

of the topmost equation in (28) yields

$$\begin{aligned}\dot{\Phi} &= P(\Phi_{\text{fp}}) - \sum_{j=1}^{N-1}\left(\frac{\alpha_j}{\kappa_j}Q_j(\Phi_{\text{fp}})\right)\\ &= R(\Phi_{\text{fp}}) = 0,\end{aligned} \tag{35}$$

where the second line is obtained using the relation (31). Therefore, (28) has a fixed point at $\begin{bmatrix}\Phi^* & \Psi_1 & \dots & \Psi_{N-1}\end{bmatrix}^T = \begin{bmatrix}\Phi_{\text{fp}} & \Psi_{1,\text{fp}} & \dots & \Psi_{N-1,\text{fp}}\end{bmatrix}^T$. For ϵ small enough, we already showed that the Jacobian of (28) evaluated at a fixed point has $N-1$ negative eigenvalues and that the sign of the remaining eigenvalue depends on the sign of $R'(\Phi_{\text{fp}})$, which is negative. Thus, the stability of these fixed points is identical.

The above analysis shows that in the weakly perturbed limit, entrainment to a periodic perturbation is identical regardless of whether operational or asymptotic phase coordinates are used. In other specific cases, these results can be extended to show, for example, that asymptotic phase locking between two oscillators is identical regardless of whether the APR or the OPR is used. As we will show in section 4.2, however, OPR is essential when trying to understand the transient behavior of a perturbed oscillator.

3. Strategy for experimental estimation of operational phase reduction. In an experimental dynamical system, such as a periodically firing neuron, it is unlikely that one would have direct access to the full dynamical equations, i.e., the right-hand side of (1). In these applications, phase reduction (2) is an attractive strategy because even without the full dynamical equations, the iPRC can be inferred using the direct method [18], [28] whereby a perturbation is given at a known phase, the measured spike time is compared to the expected spike time had the perturbation not been applied, and this procedure is repeated at multiple phases to estimate the iPRC.

Here we present a strategy for estimating the first order accurate terms of the OPR (11) using a strategy similar to the direct method. In this case, we assume that all but one isostable coordinate decays rapidly. Furthermore, we will take $G(t) = [u(t)\ 0, \dots, 0]^T$ with $u(t)$ being a perturbation to one of the state variables (for example, applying an external current to a neuron to modify its transmembrane voltage). With these assumptions, the resulting OPR will be of the form

$$\begin{aligned}\dot{\theta}^* &= \omega + \alpha_1\psi_1 + z^*(\theta^*)u(t),\\ \dot{\psi}_1 &= \kappa_1\psi_1 + i_1^*(\theta^*)u(t),\end{aligned} \tag{36}$$

where $z^*(\theta^*)$ and $i_1^*(\theta^*)$ are the first elements of $\mathcal{Z}^*(\theta^*)$ and $\mathcal{I}_1^*(\theta^*)$, respectively. Here, we will detail a strategy for obtaining all required elements ω, α_1, $z^*(\theta^*)$, κ_1, and $i_1^*(\theta^*)$ using only measurements of the transmembrane voltage and the ability to give perturbations at known times. Much like measurement of iPRCs with the direct method [18], our proposed strategy works best with many trials in order to average out the effects of random factors such as noise.

3.1. Estimation of ω and κ_1. We define the nth ISI as $\text{ISI}_n = t_{n+1}^* - t_n^*$, where t_n^* is the time of the nth spike. For a single oscillator, the estimation of ω is relatively straightforward—

by taking multiple measurements of the ISI, the unperturbed natural period can be estimated by the mean of M ISIs:

$$T = \frac{1}{M}\sum_{i=1}^{M} \mathrm{ISI}_i. \tag{37}$$

The natural frequency can be estimated as $\omega = 2\pi/T$. In order to obtain an estimate for κ_1, consider a trajectory which has been perturbed from its limit cycle so that the asymptotic phase, θ, reaches zero at some time t_0. Referring back to Figure 2, in this situation, the nth time to cross the $\theta^* = 0$ isochron can be found by substituting (18) into (16) yielding the relation

$$t_n^* = t_0 + nT - \frac{\psi_1(t_0)\lambda_1^n \alpha_1}{\omega\kappa_1}. \tag{38}$$

Using (38), one can show

$$\begin{aligned} t_{n+1}^* - t_n^* &= T + \frac{\psi_1(t_0)\alpha_1\lambda_1^n(1-\lambda_1)}{\omega\kappa_1}, \\ \log(\mathrm{ISI}_n - T) &= \log\left(\frac{\psi_1(t_0)\alpha_1(1-\lambda_1)}{\omega\kappa_1}\right) + n\log(\lambda_1). \end{aligned} \tag{39}$$

From (39), $\log(\lambda_1)$ can be obtained starting with initial condition perturbed from the limit cycle and calculating the slope of a simple linear regression of $\log(\mathrm{ISI}_n - T)$ as a function of n during its return to the limit cycle. For a noisy system, this can be repeated for multiple measurements to obtain an averaged estimate for $\log(\lambda_1)$ (see panels A and B of Figure 5, for example). Equation (50) in Appendix A gives the relation $\kappa_1 = \frac{\log(\lambda_1)}{T}$, so that κ_1 can be inferred from λ_1.

3.2. Estimation of α_1, $i_1^*(\theta^*)$, and $z^*(\theta^*)$. Here we detail a strategy for the measurement of α_1, $i_1^*(\theta^*)$, and $z^*(\theta^*)$. To begin, suppose that at some time t_p, the oscillator is on its limit cycle (i.e., $\psi_1(t_p) = 0$). We will approximate the operational phase as $\theta^*(t_p) = \theta_p^* \approx 2\pi(t_p - t_0^*)/T$, where t_0^* is the time of the last spike. Suppose that at t_p, we apply a small perturbation $u = u_p$ lasting for Δt seconds. Provided this perturbation is small enough so that the perturbed behavior is a good approximation of the asymptotic behavior, the perturbed phase will be $\theta_p^* + z^*(\theta_p^*)u_p\Delta t$ and the perturbed isostable coordinate will be $i_1^*(\theta_p^*)u_p\Delta t$. By definition, the nth spike after the perturbation will occur when θ^* reaches $2\pi n$, so that the time at the nth spike, t_n^*, solves the equation

$$\begin{aligned} 2\pi n &= \theta_p^* + \omega(t_n^* - t_p) + z^*(\theta_p^*)u_p\Delta t + \int_{t_p}^{t_n^*} \alpha_1\psi_1(t)dt \\ &= \theta_p^* + \omega(t_n^* - t_p) + z^*(\theta_p^*)u_p\Delta t + \frac{\alpha_1 u_p \Delta t}{\kappa_1} i_1^*(\theta_p^*)\left[\exp(\kappa_1(t_n^* - t_p)) - 1\right]. \end{aligned} \tag{40}$$

Here, the integral is evaluated by noting that $\psi_1(t) = \psi_1(t_p)\exp(\kappa_1(t - t_p))$. Evaluating (40) at the first and the nth spike, subtracting the difference, and rearranging yields an equation

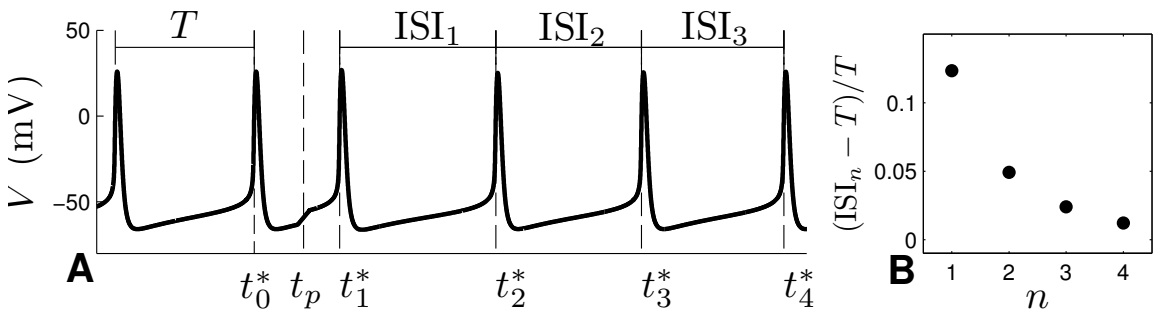

Figure 3. *Schematic of a single set of measurements required for estimation of the iPRC and iIRC for a periodically firing neuron in the absence of noise. In panel A, the oscillator is allowed to relax to its periodic orbit before a small perturbation is applied at time t_p. The measured time t_n^* gives the time of the nth spike after t_p. By only needing to measure the spike times, (40) and (41) can be used to estimate $\alpha_1 i_1^*(\theta^*)$ and $z^*(\theta^*)$. Panel B shows the ISIs relative to the natural period.*

independent of $z^*(\theta^*)$,

$$\alpha_1 i_1^*(\theta_p^*) = \frac{\kappa_1[2\pi(n-1) - \omega(t_n^* - t_1^*)]}{u_p \Delta t\big[\exp(\kappa_1(t_n^* - t_p)) - \exp(\kappa_1(t_1^* - t_p))\big]}. \tag{41}$$

After obtaining estimates for κ_1 and ω as shown in the previous section, all values on the right-hand side of (41) are known, providing a single estimate for $\alpha_1 i_1^*(\theta_p)$. Over multiple trials for different values of θ_p, allowing the oscillator to return to its limit cycle between perturbations, the resulting data can be fit with an appropriate basis (e.g., sinusoids) in order to estimate the relation $\alpha_1 i_1^*(\theta^*)$. Even though the specific values of $i_1^*(\theta^*)$ and α_1 cannot be resolved, this does not matter since a change of basis $\bar{\psi}_1 = c\psi_1$ with $\bar{i}_1^* = c i_1^*$ and $\bar{\alpha}_1 = \alpha_1/c$ does not change the dynamics (36); the product $\alpha_1 i_1^*(\theta^*)$ is all that is important. Practically, to determine the individual terms for use in (36), one can choose α_1 as convenient and scale $i_1^*(\theta^*)$ to maintain the necessary relationship.

Once the estimates α_1 and $i_1^*(\theta^*)$ have been obtained, the only unknown remaining in (40) is $z^*(\theta^*)$. Using the same spiking data that was used for the estimates from (41), we can now use (40) to get pointwise estimates of $z^*(\theta^*)$. The resulting data can be fit to a curve to calculate the operational iPRC. Figure 3 gives an illustration of the measurements required for a single estimate of both $i_1^*(\theta^*)$ and $z^*(\theta^*)$.

4. Examples.

4.1. Operational phase reduction of the isochron clock. Consider the following two-dimensional system, which is a modified version of the radial isochron clock [47]:

$$\begin{aligned} \dot{r} &= \sigma(1 - r^2)r, \\ \dot{\vartheta} &= 1 + \rho(r^2 - 1). \end{aligned} \tag{42}$$

Here, r and ϑ represent a radial and angular coordinate, respectively, and σ and ρ are constants. When σ is positive, the system admits a stable periodic orbit with $r = 1$, shown in

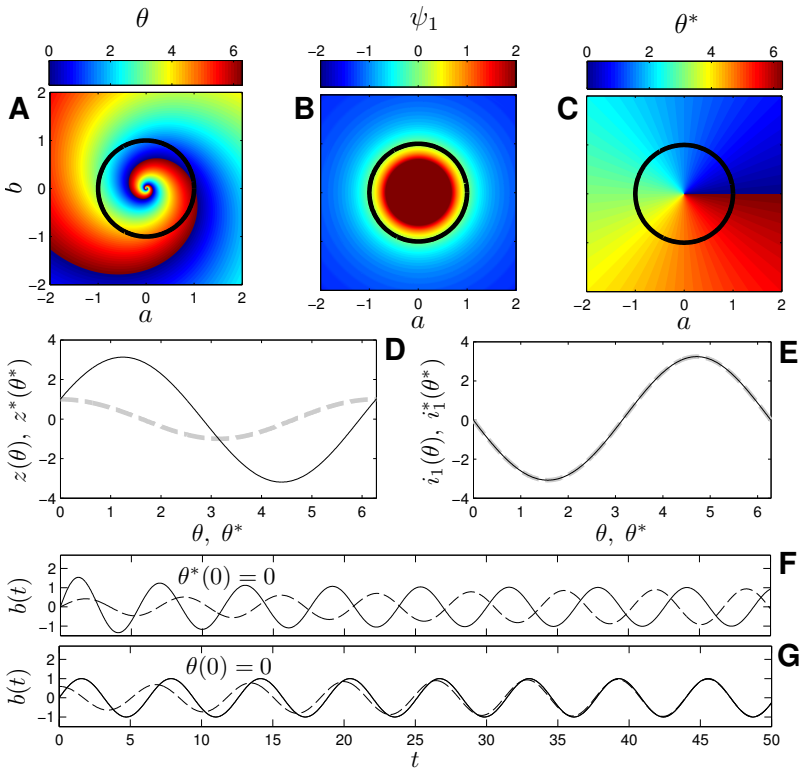

Figure 4. *Panels* A, B, *and* C *show the asymptotic phase, isostable, and operational phase coordinates, respectively, as a function of spatial location. In panels* D *and* E*, dashed gray and solid black lines show the resulting curves when using operational and asymptotic phase coordinates, respectively. In panel* E*, $i_1(\theta)$ and $i_1^*(\theta^*)$ are identical, which is consistent with the relationship derived in* (13)*. Panel* F *(resp.,* G*) shows the behavior of initial conditions for which the operational (resp., asymptotic) phase is identical at $t = 0$.*

black in panels A–C of Figure 4, and ρ determines the change in the angular rate of rotation for perturbations in the radial direction. For (42) with $\rho = 0.12$ and $\sigma = 0.04$, isochrons are calculated according to (3) and shown in panel A of Figure 4. Because $\rho \neq 0$, the isochrons spiral into the origin. The $\theta = 0$ isochron is chosen to define a Poincaré surface with numerically calculated nonunity Floquet multiplier $\lambda_1 = 0.605$ and corresponding right eigenvector $v_1^T = [0.3162, -0.9487]$ and left eigenvector $u_1^T = [3.1623, 0]$. This information is used along with the definition of isostable coordinates from (48) of Appendix A to numerically calculate the isostable coordinate ψ_1 for (42), with results shown in panel B of Figure 4. Letting $a = r\cos(\vartheta)$ $b = r\sin(\vartheta)$ define a Cartesian coordinate system, panel D (resp., panel E) shows $z(\theta) \equiv \partial\theta/\partial b$ and $z(\theta^*) \equiv \partial\theta^*/\partial b$ (resp., $i_1(\theta) = i_1^*(\theta^*) \equiv \partial\psi_1/\partial b$), where both functions are evaluated on the limit cycle.

In this example it is relatively straightforward to determine operational phase coordinates θ^* once both the asymptotic phase and isostable coordinates have been calculated. To do so, we define $\theta = 0$ to correspond to the location at which b crosses zero in the right half of the plane, i.e., the boundary between the red and blue colors in panel C of Figure 4. From (7), operational phase coordinates can be inferred by numerically estimating $D \equiv \int_0^\infty d(\psi_1)dt$

using the $\theta^* = 0$ surface. Panel C of Figure 4 shows the operational phase coordinates for this system, which extend radially from the origin. Intuitively, using the operational instead of asymptotic phase undoes the "twist" in the isochrons. In panel F, the solid and dashed lines show the behavior of two initial conditions $(a(0), b(0)) = (1.7, 0)$ and $(0.4, 0)$, respectively, chosen so that $\theta^*(0) = 0$. Analogously, solid and dashed lines in panel G show the behavior of two initial conditions $(a(0), b(0)) = (1, 0)$ and $(0, 0.594)$, respectively, chosen so that $\theta(0) = 0$. Intuitively, the operational phase coordinate provides instantaneous information about the state (i.e., $\theta^* = 0$ reflects the moment when b crosses from negative to positive values) but does not contain any information about the asymptotic behavior. Conversely, the asymptotic phase coordinate provides information about the infinite time behavior but does not contain information about the transient behavior.

4.2. Estimation of the operational phase reduction and transient behavior of a neural oscillator. Here we will calculate the OPR for the Wang–Buzsaki model [40] with adaptation given in (4). Here, we will also consider a Gaussian white noise process, $\sqrt{2D}\eta(t)$, to model general system noise and an external perturbation, $u(t)$, both added to the transmembrane voltage equation. We will calculate the terms in the first order OPR (11) in two different ways: first by numerically calculating the terms of the APR in the absence of noise and inferring the corresponding terms from (11) using (13) and (18) and, second, by estimating the terms of the phase reduction using the strategies developed in section 3. To numerically calculate the APR, the periodic orbit is found numerically to have three nonunity Floquet multipliers; we numerically calculate the Floquet multipliers $\lambda_1 = 0.527$, $\lambda_2 = 0.011$ and find that $|\lambda_3| < 10^{-5}$. Since λ_2 and λ_3 are close to zero, we will assume the isostable coordinates ψ_2 and ψ_3 are simply equal to zero. The nonzero isostable coordinate ψ_1 has the Floquet multiplier $\kappa_1 = \log(\lambda_1)/T = -0.055$. With this information, $\mathcal{Z}(\theta)$ and $\mathcal{I}_1(\theta)$ from the APR can be calculated as the appropriately normalized solution to the adjoint equation (53) (see Appendix A for details). To convert the asymptotic phase coordinates to operational phase coordinates, α_1 is calculated numerically according to (18) allowing $\mathcal{I}_1^*(\theta^*)$ and $\mathcal{Z}^*(\theta^*)$ to be calculated using (13), assuming that κ_2 and κ_3 are sufficiently large in magnitude so the contributions from $\mathcal{I}_2(\theta)$ and $\mathcal{I}_3(\theta)$ are both negligible. The response to voltage perturbations $i_1^*(\theta^*) \equiv \partial\psi_1/\partial V$ and $z^*(\theta^*) \equiv \partial\theta^*/\partial V$ are the first elements of $\mathcal{Z}^*(\theta^*)$ and $\mathcal{I}_1^*(\theta^*)$, respectively. Here, $\theta^* = 0$ is defined to be the point at which $V = 0$ and $\dot{V} > 0$ (i.e., during the transmembrane voltage upstroke of an action potential). In panels D–F of Figure 5, black curves represent the relevant functions of the OPR, calculated numerically. The relationship from (13) is used to calculate the asymptotic phase response curve.

Using the methodology developed in section 3, we also calculate the necessary terms of the OPR. We do this for two different sets of simulations for which the noise intensity $2D$ is 0.8 and 1.6. Here, we assume that we have the ability to apply a perturbation $u(t)$ and can measure the neuron's transmembrane voltage but have no other information about this neuron. When measuring the noisy ISIs, the mean converges to the unperturbed natural period of 11.74 ms, which we will use for all calculations in the direct method. Panel A of Figure 5 illustrates the strategy used for estimation of κ_1, by which a constant perturbation is applied and the neuron is given time to adapt. After adaptation occurs, the perturbation is removed immediately after a spike is detected, and the ensuing ISIs are measured. This procedure

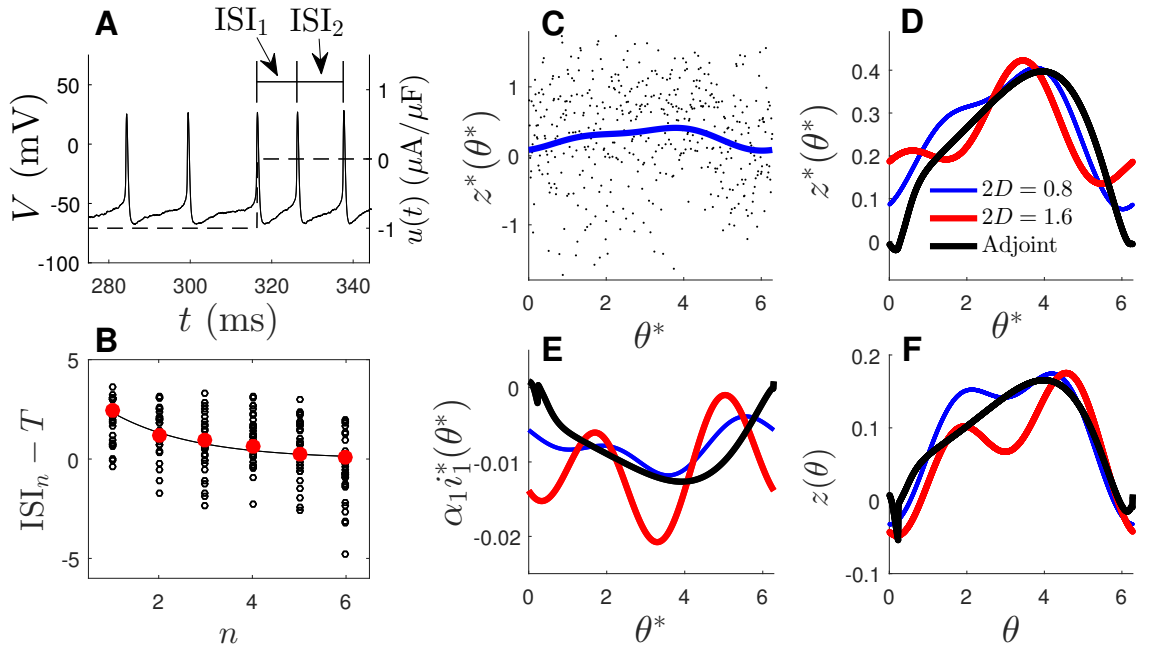

Figure 5. *Estimation of the OPR using the direct method. In panel* A*, the neuron is allowed to adapt to a hyperpolarizing (negative) perturbation. Transmembrane voltage is shown as a solid line and the perturbation is shown as a dashed line. Upon its removal, the ISIs are shorter on average during relaxation to the periodic orbit. Black circles in panel* B *show representative measurements using this procedure over multiple trials and an exponential fit to the data yields the Floquet multiplier* λ_1*. Panel C shows a subset of datapoints obtained using the procedure outlined in section* 3 *for estimation of* $z^*(\theta^*)$ *with* $2D = 0.8$*. The blue line is fit to the data. Panels* D *and* E *show estimates of the functions in the augmented phase reduction obtained using the direct method with a noisy system (blue and red lines) compared to their true values, obtained with a noiseless system using the adjoint equation (black line). Panel* F *shows the asymptotic phase response curve, inferred using* (13).

is repeated 500 times, and panel B shows a representative subset of these measurements with red dots indicating the mean values over all trials. Per (39), a linear regression of $\log(\text{ISI}_n - T)$ as a function of n yields an estimate of $\log(\lambda_1)$. An estimate of κ_1 is obtained immediately as $\log(\lambda_1)/T$. Trials with $2D = 0.8$ and 1.6 give estimates $\kappa_1 = -0.048$ and -0.060, respectively. Using the strategy detailed in section 3.2, $i_1^*(\theta^*), z^*(\theta^*)$, and α are estimated with 10,000 perturbations with alternating magnitudes $u_p = 1$ and $-1\mu\text{A}/\mu\text{F}$ with $\Delta t = 1$ ms. Panel C shows a representative subset of samples of $z^*(\theta^*)$, calculated using (40), when $2D = 0.8$. In panels D and E, the function $\sum_{n=0}^{2}[a_i \sin(n\theta^*) + b_i \cos(n\theta^*)]$ is fit to the datapoints for $z^*(\theta^*)$ and $\alpha_1 i_1^*(\theta^*)$. Constants of the fits are chosen to minimize the sum of the squared residuals. Panel F shows the asymptotic phase response curve, inferred from the terms of each OPR. In both simulations of different noise intensity, $z^*(\theta^*)$ is well approximated by this procedure. The estimates of $\alpha_1 i_1^*(\theta^*)$ are slightly less accurate, particularly as the noise intensity increases. However, the qualitative behavior is correct at both noise levels. Interestingly, the approximations of the asymptotic phase response curve (panel F) are quite robust, for larger noise intensities.

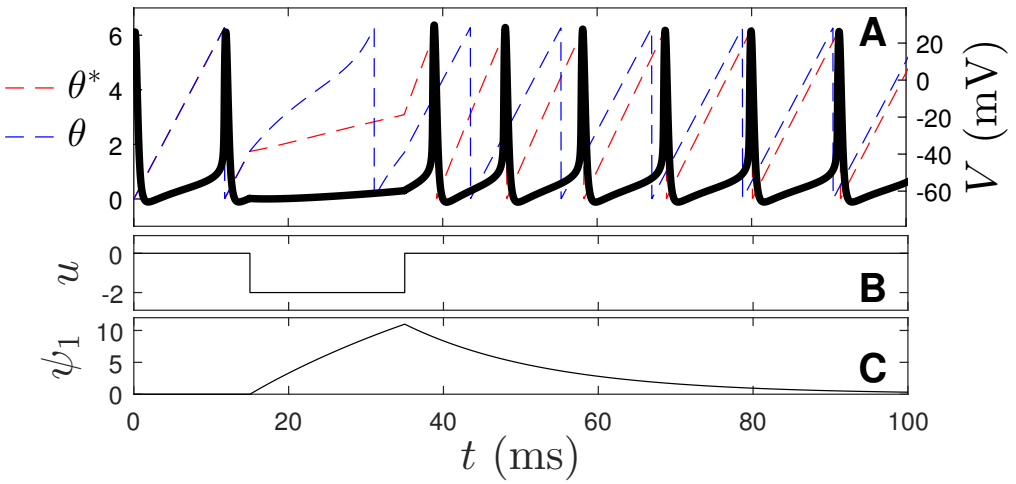

Figure 6. *Transient response of (4) to a hyperpolarizing pulse. In panel* A*, black, dashed red, and dashed blue traces show the time courses of V, θ^*, and θ, respectively. Action potentials in the full model always coincide with $\theta^* = 0$, while the APR is accurate only once the neuron has decayed to the periodic orbit. Panel* B *gives the time course of the perturbation, and panel* C *shows the rise and subsequent exponential decay of ψ_1 in response to the perturbation.*

In the implementation of the direct method shown here, noise has a significant impact on the ISI. For example, for a noise intensity of $2D = 1.6$, the variance in spike times of the unperturbed system is approximately 5 ms, about half the natural period. In order to obtain accurate measurements in this particularly noisy environment many measurements must be taken. Most likely, it would be difficult to get this amount of data in a real experiment; however, for systems where noise intensity is smaller, fewer measurements will be required to guarantee a reasonable estimate of the terms in the OPR.

As its name implies, APR is useful for predicting the infinite time behavior of a perturbed oscillator. In examples illustrated here, in addition to the asymptotic behavior, OPR predicts transient oscillatory behavior and is valid for general perturbations. First, consider the transient behavior of a neuron from (4) in response to an applied current perturbation shown in Figure 6. The black voltage trace in panel A shows the behavior of a noiseless neuron (i.e., with $2D = 0$) in response to a $u(t) = -2$ μA/μF current perturbation lasting approximately 20 ms. The blue and red traces show the predicted behavior using the APR (5) and the OPR (11), respectively. All functions and parameters of the reductions are calculated numerically with the adjoint equation (53) for a noiseless neuron (shown with black lines in panels C–E of Figure 5). In panels B and C of Figure 6, the isostable coordinate ψ_1 increases rapidly during the application of the hyperpolarizing stimulus and decays asymptotically during the subsequent relaxation to the periodic orbit. The results from Figure 6 are a clear demonstration of the ability of the OPR to capture the transient dynamics of the periodically firing neuron. Each action potential occurs at almost exactly the same moment that $\theta^* = 0$, while for the APR, the moments at which $\theta = 0$ occur as much as 8 ms in advance of the true spikes. Also notice that as ψ_1 decays and the trajectory approaches the periodic orbit, the asymptotic phase becomes a better indicator of when action potentials occur in the full model.

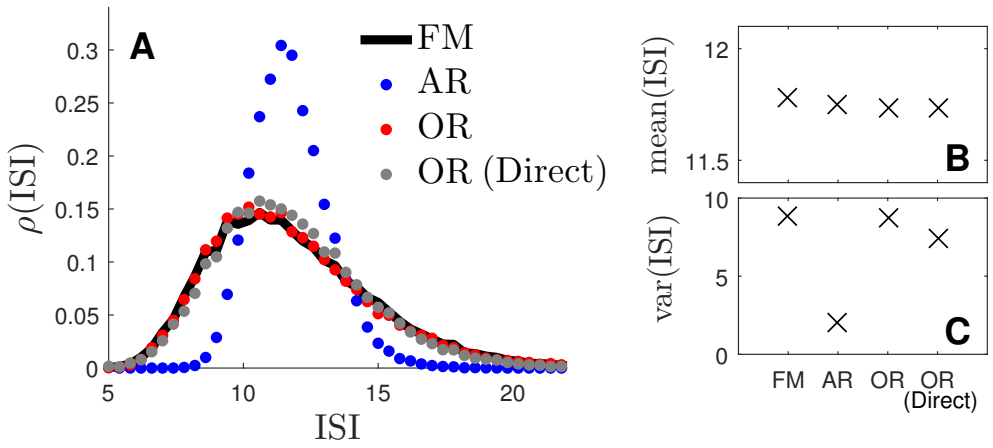

Figure 7. *The black line gives an approximate probability distribution of ISIs for simulations of over* 40,000 *spikes of the full model* (4) *with noise intensity* $2D = 4$. *Blue dots (resp., red and gray dots) give estimates using the asymptotic reduction* (43) *(resp., operational reduction* (44)*). Gray dots correspond to simulations where* $z^*(\theta^*)$ *and* $i_1^*(\theta^*)$ *are obtained from the direct method; all other reduced functions are obtained using the adjoint method. The mean and variance for each set of simulations are shown in panels* B *and* C*, respectively.*

As illustrated in Figure 6, OPR is particularly useful for predicting the transient behavior of an oscillator. This becomes particularly important if the behavior in response to perturbations never reaches a steady state. To illustrate this, consider an adapting neuron with an ISI which varies in response to white noise added to the transmembrane voltage. Here, we simulate the full equations (4) with a noise intensity $2D = 4$, along with corresponding APR and OPR, (5) and (11), respectively. Here we take $u(t) = 0$ so that the only perturbations are from noise. For the phase reduced stochastic differential equations, we assume that the noise intensity is small enough so that higher order noise terms are negligible (cf. [8], [23]) yielding

$$\dot{\theta} = \omega + z(\theta)\sqrt{2D}\eta(t) \tag{43}$$

and

$$\begin{aligned} \dot{\theta}^* &= \omega + \alpha_1\psi_1 + z^*(\theta^*)\sqrt{2D}\eta(t), \\ \dot{\psi}_1 &= \kappa_1\psi_1 + i_1^*(\theta^*)\sqrt{2D}\eta(t). \end{aligned} \tag{44}$$

In simulations of the OPR (44), we use $z^*(\theta^*)$ and $i_1^*(\theta^*)$ calculated according to the adjoint method (53), and the direct method with $2D = 1.6$ (black and red curves, respectively, from panels D and E of Figure 5). Both curves are chosen to compare results when the terms of (44) are not measured perfectly. Simulations of the APR (43) use $z(\theta)$ calculated according to the adjoint method (53). In each set of simulations, over 40,000 consecutive spikes are obtained in order to yield estimates for the ISI probability densities from panel A of Figure 7. Spiking statistics with the full model (FM) and the operational reduction (OR) calculated with the adjoint method are nearly identical. Panels B and C of Figure 7 give the mean and variance of the ISIs, respectively, for each simulation. When using the OR with noisy measurements, the results disagree slightly when compared to the full model but are still

quite similar. In contrast, the simulations with the asymptotic reduction (AR) significantly underestimate the variance in spike times. Furthermore, the asymptotic reduction simulations give an ISI distribution which appears nearly Gaussian (cf. [8]), while in all other simulations, the ISI distribution has a much longer tail extending toward larger ISIs. Qualitatively similar profiles are obtained when using smaller noise magnitudes.

5. Discussion and conclusion. While phase reduced coordinate systems using an asymptotic definition of phase are useful for understanding the behavior of complex biological oscillators, the transient behavior is not considered when working in this reduced coordinate system. Here, we propose a new coordinate system which uses an operational phase, defined relative to some meaningful event (such as the timing of a neural action potential) rather than the asymptotic behavior. The definition of operational phase proposed in this work only requires knowledge of a single state variable, making it suitable to experimental systems where the measurement of multiple variables with high temporal resolution is generally limited.

It is well documented that perturbations to periodically firing neurons can affect the timing of not only the next action potential but also subsequent action potentials [32], [29], a feature that standard phase reduction cannot accommodate. While strategies which use residual or higher order iPRCs [5], [31], [11] have been proposed to correct for this physiological phenomenon, they are generally limited to specific types of perturbations. Here, OPR tracks the decay of modes that are transverse to the periodic orbit in order to replicate this phenomenon resulting from sufficiently small but arbitrary perturbations. In certain cases, corrections to the OPR can be made to extend its accuracy at locations that are farther from the limit cycle (e.g., section 2.3), but this becomes particularly difficult as the number of nonnegligible isostable coordinates increases.

APR is a particularly attractive strategy when the full dynamical equations governing the behavior of a limit cycle oscillator are unknown, as the necessary curves can be obtained through the well-established direct method [18], [28], which is briefly summarized below. Recalling the definitions of spike times t_n^* and perturbation time t_p from Figure 3, the standard implementation of the direct method only requires t_0^*, t_1^*, and t_p to obtain an estimate of the phase response curve $z(\theta_p) = -2\pi(t_1^* - t_0^* - T)/(Tu_p\Delta t)$, where $\theta_p = 2\pi t_p/T$, and u_p and Δt are the magnitude and duration of the applied perturbation. Provided the magnitude of u_p is sufficiently small and perturbations transverse to the periodic orbit decay rapidly, it is well established that the resulting phase response curve can be used to predict the behavior of arbitrary perturbations using the phase reduced equation $\dot{\theta} = \omega + z(\theta)u(t)$ [10], a strategy which has been successfully applied in many experimental settings [21], [27], [38]. A similar strategy for direct measurement of the terms in the OPR has been proposed here. When isostable coordinates decay slowly, the OPR has the ability to predict the effect of a perturbation on the current ISI and all subsequent ISIs. The direct strategy proposed here is shown to work well provided the decay of directions transverse to the periodic orbit can be well approximated by the decay of a single isostable coordinate.

The operational phase coordinates presented here rely on the notion of isostable coordinates of periodic orbits [44], [46] which give a sense of the asymptotically exponential decay of trajectories towards a limit cycle solution. This choice of coordinates transverse to the periodic orbit is particularly effective here because the reduced dynamics decay exponentially

in the absence of perturbations, allowing for the derivation of relatively straightforward relationships between the asymptotic and operational phase coordinates in the fully nonlinear regime (7). At locations sufficiently close to the stable periodic orbit, simple relationships between operational and asymptotic phase coordinates are also obtained (10). Unlike other phase-amplitude reduction strategies [4], [41], [36], OPR is explicitly tied to an event which is easily detectable at locations farther from the limit cycle and can be implemented even when only a single state variable can be measured. In principle, many of these phase-amplitude reduction strategies could be used to detect meaningful events in the full equations without the need to introduce operational phase coordinates. This could be achieved, for instance, by determining a Poincaré section of the reduced equations which corresponds to the $\theta^* = 0$ level set of the full equations. However, the calculation of such a Poincaré section for a general nonlinear dynamical system would not be trivial.

While OPR represents a significant advance in the study of the transient behavior of limit cycle oscillators, the methods presented here can still be improved upon. Perhaps most notably, in an experimental setting, the direct measurement strategy of the terms of the OPR presented here requires that the transient dynamics can be accurately captured by a single isostable coordinate. It would certainly be of interest to develop strategies to accurately measure the terms in the OPR when multiple isostable coordinates contribute to the transient behavior. Such a strategy would most likely require knowledge of additional state variables in the nonlinear system. Experimentally, these additional measurements might be obtained either through simultaneous measurement or by using techniques for inferring the other state variables [16], [39]. Also, the operational phase reduced coordinates presented here are defined using a single event to explicitly define the location at which $\theta^* = 0$. It would be interesting to investigate the effects of incorporating multiple explicit definitions in a slightly different set of reduced coordinates. As a concrete example in a spiking neuron, θ_1^* might correspond to the timing of an action potential and θ_2^* might correspond to a particular feature tied to the calcium dynamics.

The OPR presented here allows for greater understanding of the transient behavior of limit cycle oscillators for which perturbations transverse to the periodic orbit do not decay rapidly. The transient dynamics of perturbed oscillators are an important feature in many biological applications. For instance, circadian misalignment (jet lag) results from a sudden perturbation to the time of one's circadian day, with symptoms lasting until one's circadian rhythms can reentrain to the new light-dark cycle [12], [34]. Furthermore, the complex interactions leading to transient hypersynchronous behavior among neurons during seizures [19], [13] could be useful to model using an OPR. Preliminary numerical simulations suggest that the effect of noise on the spike times of oscillatory neurons could be well understood using OPR. For example, Figure 7 show non-Gaussian distributions of ISIs in an adapting neural oscillator subject to additive Gaussian white noise. These results are different from those which use APR [8], [26]. Future work may be devoted to understanding the behavior of these systems which result in more complicated distributions of spiking intervals.

Appendix A. Isostable coordinates and augmented phase reduction. Here we give a brief overview of the important features of augmented phase reduction as described in [44] (cf. [46]). The isostable coordinates used here were inspired by the notion of isostables set

forth in [25] to characterize the approach of a trajectory to a stable equilibrium solution. To start, consider the stable periodic orbit, γ, of the ordinary differential equation (1). If we define Γ_0 as the $\theta = 0$ isochron, then recalling the definition of isochrons (3), this initial condition will first return to Γ_0 at time T, where T is the natural period. This allows us to define Γ_0 as a Poincaré surface and the associated Poincaré map

$$P : \Gamma_0 \to \Gamma_0, \tag{45}$$

$$x \mapsto \varphi(T, x), \tag{46}$$

where φ is the unperturbed flow of the system. Note that this map has a stable fixed point $P(x_0) = x_0$ for x_0 on γ and $\theta(x_0) = 0$. We can approximate the solution of this map near the fixed point as

$$\varphi(T, x) = x_0 + J_P(x - x_0) + \mathcal{O}(||x - x_0||^2), \tag{47}$$

where J_p is the Jacobian of $\varphi(T, x)$ evaluated at x_0. For each real, semisimple (i.e., with identical algebraic and geometric multiplicity) eigenvalue λ_i of J_p, consider the corresponding left and right eigenvectors u_i and v_i, respectively. We can define isostable coordinates provided $|\lambda_i| < 1$ as follows (cf. [44]):

$$\psi_i(x) = \lim_{j\to\infty} \big[\underbrace{u_i^T(\varphi(t_\Gamma^j, x) - x_0)}_{g_i(x,t)} \underbrace{\exp(-\log(\lambda_i)t_\Gamma^j/T)}_{h_i(x,t)} \big], \tag{48}$$

where t_Γ^j is the jth return time to Γ_0 under the flow. In the above definition, the sequence $\{\varphi(t_\Gamma^j, x)\}_{j\in\mathbb{N}}$ approaches x_0 so that for j large enough, its convergence is well approximated by

$$\varphi(t_\Gamma^j, x) - x_0 = \sum_{j=1}^{N} (s_j(x) v_j \lambda^j), \tag{49}$$

where s_j are coordinates in the basis of eigenvectors of J_p. Note that (49) is only valid in the limit as time approaches infinity so that the dynamics can be well approximated by a linearization about the fixed point. The left eigenvector u_i in (48) is used to select for the component of (49) in the v_i direction and the resulting term $g_i(x, t)$ shrinks at a rate λ_i. Considering the term $h_i(x, t)$, because the trajectory crosses the Poincaré section every T units of time, it grows at a rate $1/\lambda_i$. The resulting multiplication $g_i(x, t)h_i(x, t)$ approaches a constant as j approaches infinity, yielding the isostable coordinate $\psi_i(x)$. Using (48) isostable coordinates are defined for all locations in the basin of attraction of the limit cycle, not just on the Poincaré section.

While the definition of isostable coordinates is somewhat complicated, their behavior is quite simple; one can show (cf. [44]) that when $G(t) = 0$, $d\psi_i/dt = \kappa_i\psi_i$, where

$$\kappa_i = \log(\lambda_i)/T, \tag{50}$$

so that isostable coordinates decay exponentially. Furthermore, as shown in [44], for $\mathcal{O}(\epsilon)$ perturbations to the limit cycle, there is a one-to-one correspondence between isostable coordinates and the state of a system to leading order ϵ given by

$$x = x^{\gamma}(\theta) + \sum_{i=1}^{N-1} p_i(\theta(t))\psi_i,$$

$$p_i(\theta(t)) = \frac{[\varphi(\theta/\omega, \epsilon v_i + x_0) - \varphi(\theta/\omega, x_0)]\exp(-\kappa_i\theta/\omega)}{\epsilon}, \tag{51}$$

where $x^{\gamma}(\theta)$ represents the state on γ as a function of the phase, $p_i(\theta)$ relates the isostable coordinate ψ_i to a corresponding perturbation from the limit cycle, $\omega = 2\pi/T$, and $t = \theta/\omega$. Furthermore, this coordinate system can be used to define a second order accurate phase and isostable reduction of the following form:

$$\dot{\theta} = \omega + \left[\mathcal{Z}(\theta)^T + \sum_{j=1}^{N-1} \left(\psi_j \mathcal{B}_j(\theta)^T\right)\right] G(t),$$

$$\dot{\psi}_i = \kappa_i\psi_i + \left[\mathcal{I}_i(\theta)^T + \sum_{j=1}^{N-1} \left(\psi_j \mathcal{D}_j^i(\theta)^T\right)\right] G(t),$$

$$i = 1, \ldots, N-1, \tag{52}$$

where $\mathcal{Z}(\theta) \equiv \frac{\partial\theta}{\partial x}|_{x^{\gamma}(\theta)}$, $\mathcal{I}_i(\theta) \equiv \frac{\partial\psi_i}{\partial x}|_{x^{\gamma}(\theta)}$, $\mathcal{B}_i(\theta) \equiv (\frac{\partial}{\partial\psi_i}\frac{\partial\theta}{\partial x})|_{x^{\gamma}(\theta)}$, and $\mathcal{D}_j^i(\theta) \equiv (\frac{\partial}{\partial\psi_j}\frac{\partial\psi_i}{\partial x})|_{x^{\gamma}(\theta)}$. Recalling from the main text that ψ_i and $G(t)$ are both $\mathcal{O}(\epsilon)$ terms, truncation of the $\mathcal{O}(\epsilon^2)$ terms from (52) yields the first order reduction (5). In order to calculate the functions $\mathcal{Z}(\theta)$ and $\mathcal{I}_i(\theta)$ numerically a useful strategy is to use the adjoint equation [9], [2]. To apply this strategy, one can choose any initial condition in γ to correspond to $\theta = 0$. After making this choice, the phase and isostable response curves, $d\theta/dx|_{x(t)} \equiv \nabla_{x(t)}\theta$ and $d\psi_i/dx|_{x(t)} \equiv \nabla_{x(t)}\psi_i$, are the periodic solutions to

$$\frac{d\nabla_{x(t)}\theta}{dt} = -J(x(t))^T\nabla_{x(t)}\theta,$$

$$\frac{d\nabla_{x(t)}\psi_i}{dt} = \left[\kappa_i I - J(x(t))^T\right]\nabla_{x(t)}\psi_i, \tag{53}$$

where $J(x(t))$ is the Jacobian of F evaluated at $x(t)$. The periodic functions $\mathcal{Z}(\theta)$ and $\mathcal{I}_i(\theta)$ are subject to the normalizing conditions $F(x(t))^T Z(\theta) = \omega$ and $v_i^T\mathcal{I}_i(0) = 1$. The functions $B_i(\theta)$ and $D_j^i(\theta)$ can be calculated by a method proposed in [44], which first requires the computation of the Hessian matrix of second derivatives of phase and isostable coordinates evaluated on the periodic orbit and then uses this information to compute the necessary functions.

Appendix B. Wang–Buzsaki model. The equations and parameters for the Wang–Buzsaki model [40] from (4) with an adaptation current [7] are given below:

$$
\begin{aligned}
C\dot{V} &= -g_{\mathrm{Na}} m_\infty^3 h(V - E_{\mathrm{Na}}) - g_{\mathrm{K}} n^4 (V - E_K) - g_{\mathrm{L}}(V - E_{\mathrm{L}}) - I_w + I_{\mathrm{b}},\\
\dot{h} &= \gamma\left[\alpha_h(V)(1-h) - \beta_h(V)h\right],\\
\dot{n} &= \gamma\left[\alpha_n(V)(1-n) - \beta_n(V)n\right],\\
\dot{w} &= a(1.5/(1+\exp((b-V)/k)) - w). \qquad (54)
\end{aligned}
$$

Here, V represents the transmembrane voltage, gating variables are denoted by h and n, and w determines the adaptation current I_w. The baseline current $I_b = 5\mu\mathrm{A}/\mu\mathrm{F}$, capacitance $C = 1\mu\mathrm{F}/\mathrm{cm}^2$, with additional equations:

$$
\begin{aligned}
m_\infty &= \alpha_m(V)/(\alpha_m(V) + \beta_m(V)),\\
\beta_n(V) &= 0.125\exp(-(V+44)/80),\\
\alpha_n(V) &= -0.01(V+34)/(\exp(-0.1(V+34)) - 1),\\
\beta_h(V) &= 1/(\exp(-0.1(V+28)) + 1),\\
\alpha_h(V) &= 0.07\exp(-(V+58)/20),\\
\beta_m(V) &= 4\exp(-(V+60)/18),\\
\alpha_m(V) &= -0.1(V+35)/(\exp(-0.1(V+35)) - 1).
\end{aligned}
$$

Reversal potentials and conductances are

$$
\begin{aligned}
E_{\mathrm{Na}} &= 55\mathrm{m}V,\\
E_{\mathrm{K}} &= -90\mathrm{m}V,\\
E_{\mathrm{L}} &= -65\mathrm{m}V,\\
g_{\mathrm{Na}} &= 35\mathrm{mS}/\mathrm{cm}^2,\\
g_{\mathrm{K}} &= 9\mathrm{mS}/\mathrm{cm}^2,\\
g_{\mathrm{L}} &= 0.1\mathrm{mS}/\mathrm{cm}^2.
\end{aligned}
$$

We take $\gamma = 5$. The adaptation current is given by

$$
I_w = g_w w(V - E_{\mathrm{K}})
$$

with associated parameters:

$$
\begin{aligned}
a &= 0.02\ \mathrm{ms}^{-1},\\
b &= -5\ \mathrm{m}V,\\
k &= 0.5\mathrm{m}V,\\
g_w &= 2\mathrm{mS}/\mathrm{cm}^2.
\end{aligned}
$$

REFERENCES

[1] M. Ainsworth, S. Lee, M. O. Cunningham, R. D. Traub, N. J. Kopell, and M. A. Whittington, *Rates and rhythms: A synergistic view of frequency and temporal coding in neuronal networks*, Neuron, 75 (2012), pp. 572–583.

[2] E. Brown, J. Moehlis, and P. Holmes, *On the phase reduction and response dynamics of neural oscillator populations*, Neural Comput., 16 (2004), pp. 673–715.

[3] G. Buzsáki and A. Draguhn, *Neuronal oscillations in cortical networks*, Science, 304 (2004), pp. 1926–1929.

[4] O. Castejón, A. Guillamon, and G. Huguet, *Phase-amplitude response functions for transient-state stimuli*, J. Math. Neurosci., 3 (2013), 13.

[5] J. Cui, C. C. Canavier, and R. J. Butera, *Functional phase response curves: A method for understanding synchronization of adapting neurons*, J. Neurophysiol., 102 (2009), pp. 387–398.

[6] J. W. Demmel, *Applied Numerical Linear Algebra*, SIAM, Philadelphia, 1997.

[7] B. Ermentrout, *Linearization of F-I curves by adaptation*, Neural Comput., 10 (1998), pp. 1721–1729.

[8] G. B. Ermentrout, B. Beverlin II, T. Troyer, and T. I. Netoff, *The variance of phase-resetting curves*, J. Comput. Neurosci., 31 (2011), pp. 185–197.

[9] G. B. Ermentrout and N. Kopell, *Multiple pulse interactions and averaging in systems of coupled neural oscillators*, J. Math. Biol., 29 (1991), pp. 195–217.

[10] G. B. Ermentrout and D. H. Terman, *Mathematical Foundations of Neuroscience*, Interdiscip. Appl. Math. 35, Springer, New York, 2010.

[11] J. Foss and J. Milton, *Multistability in recurrent neural loops arising from delay*, J. Neurophysiol., 84 (2000), pp. 975–985.

[12] D. A. Golombek and R. E. Rosenstein, *Physiology of circadian entrainment*, Physiol. Rev., 90 (2010), pp. 1063–1102.

[13] L. B. Good, S. Sabesan, S. T. Marsh, K. Tsakalis, D. Treiman, and L. Iasemidis, *Control of synchronization of brain dynamics leads to control of epileptic seizures in rodents*, Int. J. Neural Syst., 19 (2009), pp. 173–196.

[14] J. Guckenheimer, *Isochrons and phaseless sets*, J. Math. Biol., 1 (1975), pp. 259–273.

[15] J. Guckenheimer and P. Holmes, *Nonlinear Oscillations, Dynamical Systems, and Bifurcations of Vector Fields*, Appl. Math. Sci. 42, Springer, New York, 1983.

[16] M. J. Hoffman, N. S. LaVigne, S. T. Scorse, F. H. Fenton, and E. M. Cherry, *Reconstructing three-dimensional reentrant cardiac electrical wave dynamics using data assimilation*, Chaos, 26 (2016), 013107.

[17] F. C. Hoppensteadt and E. M. Izhikevich, *Weakly Connected Neural Networks*, Springer, New York, 1997.

[18] E. M. Izhikevich, *Dynamical Systems in Neuroscience: The Geometry of Excitability and Bursting*, MIT Press, London, 2007.

[19] P. Jiruska, M. D. Curtis, J. G. R. Jefferys, C. A. Schevon, S. J. Schiff, and K. Schindler, *Synchronization and desynchronization in epilepsy: Controversies and hypotheses*, J. Physiol., 591 (2013), pp. 787–797.

[20] T. Kato, *Perturbation Theory for Linear Operators*, Springer, Berlin, 1995.

[21] I. Z. Kiss, C. G. Rusin, H. Kori, and J. L. Hudson, *Engineering complex dynamical structures: Sequential patterns and desynchronization*, Science, 316 (2007), pp. 1886–1889.

[22] Y. Kuramoto, *Chemical Oscillations, Waves, and Turbulence*, Springer, Berlin, 1984.

[23] C. Ly and G. B. Ermentrout, *Synchronization dynamics of two coupled neural oscillators receiving shared and unshared noisy stimuli*, J. Comput. Neurosci., 26 (2009), pp. 425–443.

[24] S. K. Maran and C. C. Canavier, *Using phase resetting to predict* $1:1$ *and* $2:2$ *locking in two neuron networks in which firing order is not always preserved*, J. Comput. Neurosci., 24 (2008), pp. 37–55.

[25] A. Mauroy, I. Mezić, and J. Moehlis, *Isostables, isochrons, and Koopman spectrum for the action–angle representation of stable fixed point dynamics*, Phys. D, 261 (2013), pp. 19–30.

[26] J. Moehlis, *Improving the precision of noisy oscillators*, Phys. D, 272 (2014), pp. 8–17.

[27] A. Nabi, T. Stigen, J. Moehlis, and T. Netoff, *Minimum energy control for* in vitro *neurons*, J. Neural Eng., 10 (2013), 036005.

[28] T. Netoff, M. A. Schwemmer, and T. J. Lewis, *Experimentally estimating phase response curves of neurons: Theoretical and practical issues*, in Phase Response Curves in Neuroscience, Springer, New York, 2012, pp. 95–129.
[29] T. I. Netoff, C. D. Acker, J. C. Bettencourt, and J. A. White, *Beyond two-cell networks: Experimental measurement of neuronal responses to multiple synaptic inputs*, J. Comput. Neurosci., 18 (2005), pp. 287–295.
[30] T. I. Netoff, M. I. Banks, A. D. Dorval, C. D. Acker, J. S. Haas, N. Kopell, and J. A. White, *Synchronization in hybrid neuronal networks of the hippocampal formation*, J. Neurophysiol., 93 (2005), pp. 1197–1208.
[31] S. A. Oprisan, A. A. Prinz, and C. C. Canavier, *Phase resetting and phase locking in hybrid circuits of one model and one biological neuron*, Biophys. J., 87 (2004), pp. 2283–2298.
[32] A. J. Preyer and R. J. Butera, *Neuronal oscillators in aplysia californica that demonstrate weak coupling in vitro*, Phys. Rev. Lett., 95 (2005), 138103.
[33] A. D. Reyes and E. E. Fetz, *Two modes of interspike interval shortening by brief transient depolarizations in cat neocortical neurons*, J. Neurophysiol., 69 (1993), pp. 1661–1672.
[34] R. L. Sack, D. Auckley, R. R. Auger, M. A. Carskadon, K. P. Wright, Jr., M. V. Vitiello, and I. V. Zhdanova, *Circadian rhythm sleep disorders: Part* I*, basic principles, shift work and jet lag disorders*, Sleep, 30 (2007), pp. 1460–1483.
[35] J. A. Sanders, F. Verhulst, and J. Murdock, *Averaging Methods in Nonlinear Dynamical Systems*, 2nd ed., Springer, New York, 2007.
[36] S. Shirasaka, W. Kurebayashi, and H. Nakao, *Phase-amplitude reduction of transient dynamics far from attractors for limit-cycling systems*, Chaos, 27 (2017), 023119.
[37] F. H. Sieling, S. Archila, R. Hooper, C. C. Canavier, and A. A. Prinz, *Phase response theory extended to nonoscillatory network components*, Phys. Rev. E, 85 (2012), 056208.
[38] R. Snari, M. R. Tinsley, D. Wilson, S. Faramarzi, T. I. Netoff, J. Moehlis, and K. Showalter, *Desynchronization of stochastically synchronized chemical oscillators*, Chaos, 25 (2015), 23116.
[39] G. Ullah and S. J. Schiff, *Tracking and control of neuronal Hodgkin-Huxley dynamics*, Phys. Rev. E, 79 (2009), 040901.
[40] X. J. Wang and G. Buzsáki, *Gamma oscillation by synaptic inhibition in a hippocampal interneuronal network model*, J. Neurosci., 16 (1996), pp. 6402–6413.
[41] K. C. A. Wedgwood, K. K. Lin, R. Thul, and S. Coombes, *Phase-amplitude descriptions of neural oscillator models*, J. Math. Neurosci., 3 (2013), 2.
[42] S. Wiggins, *Introduction to Applied Nonlinear Dynamical Systems and Chaos*, Vol. 2, Springer, New York, 2003.
[43] C. Wilson, B. Beverlin II, and T. Netoff, *Chaotic desynchronization as the therapeutic mechanism of deep brain stimulation*, Front. Syst. Neurosci., 5 (2011), 50.
[44] D. Wilson and B. Ermentrout, *Greater accuracy and broadened applicability of phase reduction using isostable coordinates*, J. Math. Biol., 76 (2018), pp. 37–66.
[45] D. Wilson and J. Moehlis, *Clustered desynchronization from high-frequency deep brain stimulation*, PLoS Comput. Biol., 11 (2015), e1004673.
[46] D. Wilson and J. Moehlis, *Isostable reduction of periodic orbits*, Phys. Rev. E, 94 (2016), 052213.
[47] A. Winfree, *The Geometry of Biological Time*, 2nd ed., Springer, New York, 2001.